Barbara D.G. Sepulveda, Phillip Visintin and Deric J. Oehlers

Quantifying the fatigue material properties of UHPFRC with steel microfibers at cracks

Journal of Structural Engineering, 2021; 147(6):04021076-1-04021076-17

Quantifying the fatigue material properties of UHPFRC with steel microfibres at cracks

[1] Sepulveda, B.D.G., [2]Visintin, P., and [3]Oehlers, D.J.

Sepulveda, B.D., Visintin, P. and Oehlers, D.J., 2021. Quantifying the Fatigue Material Properties of UHPFRC with Steel Microfibers at Cracks. *Journal of Structural Engineering*, *147*(6), p.04021076.

Published version of manuscript available at: https://doi.org/10.1061/(ASCE)ST.1943-541X.0003051

Abstract

The addition of steel fibres to concrete in ultra-high performance concrete (UHPC) to form ultra-high performance fibre reinforced concrete (UHPFRC) has been shown to have a great benefit by substantially increasing the flexural capacities and ductilities at the ultimate limit state and reducing crack widths and increasing flexural rigidities at the serviceability limit state. This is because the fibres bridge a crack and consequently allow tensile stresses across the crack. Tests have also shown that tensile cyclic loads applied across a crack can reduce these benefits by allowing the crack to widen through a gradual debonding of the fibres. To quantify the behaviour of UHPFRC post cracking, the fatigue behaviour of steel microfibre concrete at a crack is studied through 33 tensile fatigue tests on precracked UHPFRC and 6 monotonic tests. An approach for processing the results based on the increase in crack width per cycle, that is the incremental set, has been developed and can be applied to any UHPFRC that exhibits debonding. Three distinct cyclic behaviours have been identified and quantified: where there is no incremental set such that there is no quantifiable damage due to cyclic loading; where the incremental set is constant such that there is quantifiable damage; and where there is rapid unstable increase in the incremental set.

Introduction

The superior strength and ductility and durability of ultra-high performance fibre reinforced concrete (UHPFRC) allows for elements that are more slender, lighter, stronger, less brittle, which require less maintenance (Abbas et al. 2016; Azmee and Shafiq 2018; Sohail et al. 2018). These benefits make UHPFRC attractive for use in structures such as bridges, which require long lifespans and have high ongoing maintenance requirements (Azmee and Shafiq 2018; Russell and Graybeal 2013; Voo et al. 2015). The significant post cracking tensile response of UHPFRC has further led to the suggestion that UHPFRC structural elements may be designed with significantly reduced, or even no, traditional tensile reinforcement (Yang et al. 2010). Adequate performance in bridge structures, and the potential to reduce the volume of traditional reinforcement both rely of the post-cracking tensile response of the fibres not being significantly influenced by the cyclic loads that occur as a normal part of in-service loading, that is, high cycle fatigue.

Previous high cycle fatigue tests conducted under both direct tensile loads (Isojeh et al. 2017; Makita and Brühwiler 2014; Zhang et al. 2000) and on flexural prisms (Carlesso et al. 2019; Germano et al. 2016; González et al. 2018; Naaman and Hammoud 1998) have shown that fatigue loading leads to the propagation of microcracks, which, depending on the range of stresses applied may limit the strength of the material. Consequently the tensile fatigue response of fibre reinforced concrete cannot be ignored in design (Carlesso et al. 2019; Lee and Barr 2004). While the fatigue behaviour of conventional concrete has been broadly investigated (Comité Euro-International du Béton (CEB) 1996), much less is known about the performance of fibre reinforced concretes (FRC) of all strength grades, but particularly UHPFRC.

For example, direct tension tests were performed by Zhang et al. (2000) using prismatic shaped direct tension specimens with dimensions of 60 mm x 50 mm x 55 mm manufactured from normal strength FRC with 1% steel fibres. The tests were conducted under displacement control between defined crack widths and demonstrated that a reduction in load and stiffness occurred between each cycle. Also considering normal strength FRC, Isojeh et al. (2017) conducted experimental tests using dog-bone specimens (500mm x 200 mm x 70 mm) with different amount of fibres (0.75% and 1.5%). In these tests a high peak stress was applied (between 75% and 90% of the monotonic average), and the fatigue life was found to increase with increasing fibre volume. For UHPFRC, Makita and Brühwiler (2014) conducted direct tension fatigue test on 39 UHPFRC dogbone shaped specimens with 3% fibre volume and a cross section of 40 mm x 150 mm to quantify the impact of the degree of cracking at the commencement of cycling on the endurance limit. In these tests it was observed that the fatigue limit of 10 million cycles could be reached regardless of the state of cracking prior to the commencement of fatigue loading.

In addition to these direct tension tests, a number of studies have considered the fatigue response of normal strength FRC and high strength FRC using flexural prisms. For example, Germano et al. (2016) conducted tests notched flexural prisms manufactured using normal strength concrete with either 0.5% or 1% fibre volume. From these tests it was identified that the fatigue life is highly dependent on the rate of increase of the crack opening per cycle as well as the range of cyclic loading and the load at the peak of each cycle. González et al. (2018) tested high strength FRC with the three-bending test to study the residual tensile strength after fatigue loading on both uncracked and pre-cracked specimens. The results of these tests indicated that the monotonic stress crack width relationship represents an envelope to the strength of the specimen regardless of fatigue loading and the state of cracking at which fatigue loading commences. Carlesso et al. (2019) also studied the fatigue behaviour of high strength FRC using a pre-cracked notched prism. The results of these 21 tests also showed that the monotonic stress crack width behaviour represents an envelope that can be used to predict residual strength.

Importantly, from this review of literature it can be observed that very few studies directly consider the tensile response using direct tension specimens. This is important because previous research (Cornelissen 1984) has shown that the results obtained from direct tension fatigue tests do not correspond with the results obtained from flexural tension tests, and flexural tension tests will over predict fatigue life because of the redistribution of stresses that can occur. Further, of the direct tension tests conducted to date the specimen size is often small in comparison to the fibre length, this is important because, as noted by Naaman and Hammoud (1998), a small specimen size relative to fibre length may significantly influences the tensile response due to a non-representative distribution of fibres as a result of edge effects.

To address these issues, in this work the results of a series of direct tensile fatigue tests on UHPFRC cast to have a relatively large cross section is presented. The tests required to extract the fatigue properties are first described. This is then followed by the methods of extracting the fatigue properties in a form that can be used to simulate the interaction between the monotonic and cyclic behaviours. An example is then given on using these properties to predict the behaviour of UHPFRC cracks subjected to both axial displacements and cyclic loads.

Tension specimens

Tension specimen details

The tension specimens consisted of 100 mm x 100 mm x 300 mm concrete prisms cast around 16mm bars as in Fig. 1, and which had a central test region which was unreinforced. The concrete mix had the following proportions by weight: cement 1; sand 1; silica fume 0.266;

water 0.190; superplasticiser 0.0450, high strength steel micro fibre (2% of volume) 0.163 that had a fibre length 13mm and a fibre diameter 0.2mm. At the time of testing: the concrete cylinder strength f_c remained at 166 MPa; and the concrete moduli E_c ranged from 44.9 to 47.2 GPa. After curing a saw cut was made as shown in Fig. 1(a) to induce cracking on loading. The distance from the rebar tip to the saw cut and the consequential cracked plane is 50mm which is greater than 3 times the length of a fibre so that the rebar is unlikely to affect the fibres crossing the crack. As a result of notching the specimen a single crack is formed along the height of the test specimen. To show the behaviour of the concrete when un-notched, dogbone tests were conducted at the beginning of the test period and show the material strain-hardens. A description of the un-notched tests and the results of these tests can be found in the supplementary material.

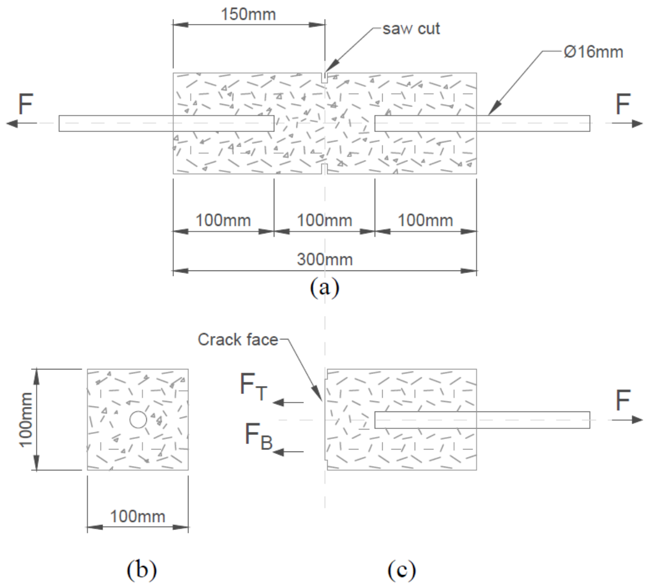

Fig. 1 Tension specimen

The specimens were subjected to the axial tensile forces F in Fig. 1(a), as shown in the test rig in Fig. 2(a). The crack width was measured with the four transducers located adjacent to the corners. A cross-section through the cracked plane in Fig. 1 is shown in Fig. 2(b) where the transducers adjacent to the corners have been labelled NW to SW. The cracked face is approximately 80 mm x 80 mm square. The dimensions shown are typical dimensions as they were measured for each individual specimen after testing and used to determine: the total cross-sectional area of the cracked plane $A_{cr\text{-}pl}$; the deformations or crack widths at the four corner of the cracked plane w_{crn}; and the crack width at the centre of the cracked plane that is the average crack width w.

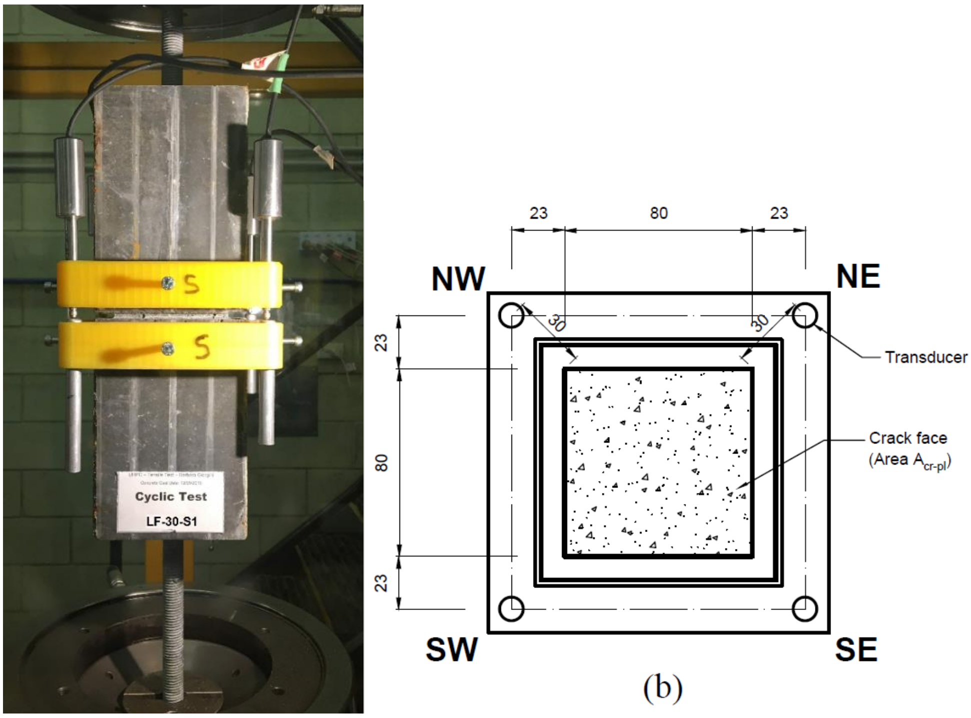

Fig. 2 (a) tension specimen test, (b) cross section of the specimen test region

Method of testing tension specimens

Ideally, the specimen in Fig. 2(a) should be tested by applying a uniform displacement across the crack face to determine the stress/crack-width relationship. However, applying appropriate restraints is difficult with this type of specimen. Alternatively, the forces F in Fig. 1 could be applied through pinned joints which would ensure a uniform distribution of stress, that is the force in the top half F_T equals the force in the bottom half F_B. However, this would not ensure a uniform crack width; for example, should F_B be less than F_T when there is a uniform crack width, then the crack width in the lower half would have to increase until there was equilibrium.

Furthermore when there is a pinned joint, failure occurs at double the strength of the weaker of the two halves so that the failure load is a lower bound to the strength.

A third approach used in this paper is to apply the forces F in Fig. 1 through fixed joints. This does not ensure a uniform crack width nor a uniform stress distribution, as it is difficult to align the applied forces, but it does ensure failure at the strength of the whole section. This approach is unsatisfactory when dealing with the deformations associated with the material strains in uncracked concrete. However it was felt that, as the deformations across the crack are orders of magnitude larger than those due to strains in the initially uncracked concrete, the fibres crossing the cracked plane could accommodate this non-alignment much better. The development of the crack across the crack face can be seen in Fig. 3 where the crack starts on the right hand side in Fig. 3(a) and propagates to the left in Figs. 3(b) and 3(c).

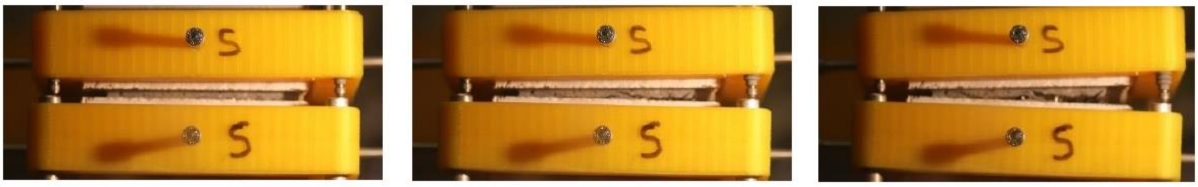

(a) (b) (c)

Fig. 3 Crack development across crack face

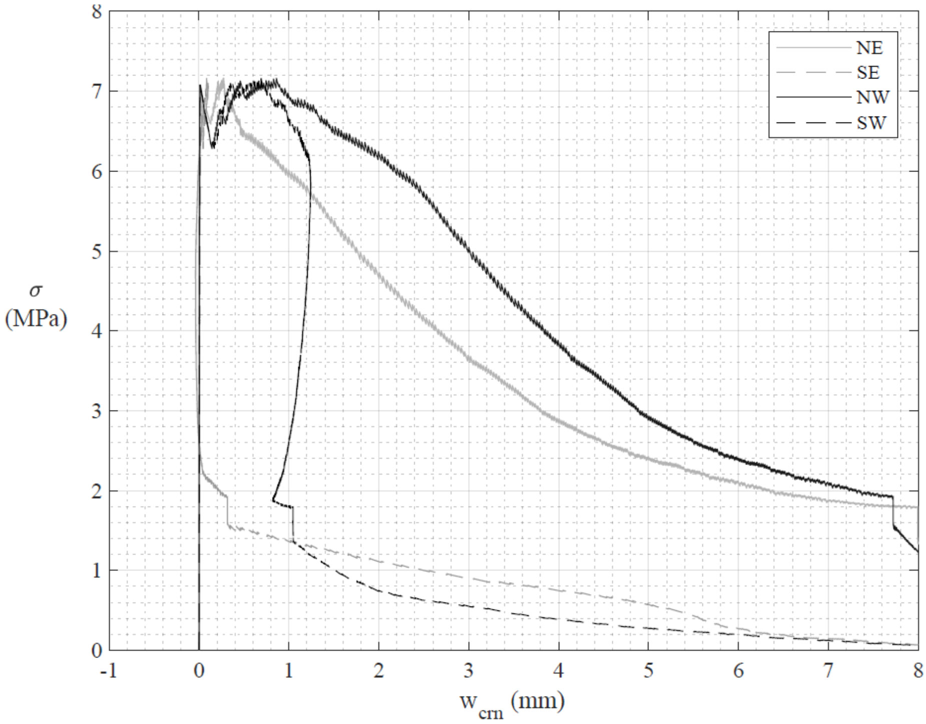

Fig. 4 Typical deformations during monotonic test

This non-alignment is further illustrated in Fig. 4 where the crack widths at the four corners of the cracked plane, during a monotonic test under displacement control, are plotted. Prior to cracking, there is no discernible crack width as would be expected, so the loading path is vertical above zero crack width. Cracking then starts at the average axial stress in the uncracked face which is recorded as f_{ctsp} which, due to the non-alignment, is a lower bound to the tensile strength of the concrete. Being under displacement control, the applied load reduces after the start of cracking. The fibres then start to take stress so that the axial force increases until it reaches a maximum where the applied load is resisted solely by the fibres. This maximum load divided by the cross-section of the cracked face will be referred to as the crack face strength f_{fi} and the average crack width at which this occurs is recorded as w_{ffi}. It can be seen in Fig. 4 that the specimen pivots about the SE corner as it only shows a discernible crack width at this corner when the applied load has reduced considerably.

Test series

Six monotonic tests were performed and their material properties are given in Table 1. The specimens are labelled MS1 to MS6, where M refers to 'monotonic' and S to 'specimen'. The cross-sectional area of the cracked face A_{cr-pl}, that was measured after the test had been completed, is listed. This is followed by what may be considered to be the material properties which were obtained using standard cylinder tests on specimens with a diameter of 100 mm and length of 200 mm and in which the reported f_c and E_c are averages obtained from 3 tests conducted in each series. This is followed by the material properties from tests on the tension specimens that is: the tensile strength at first cracking f_{ctsp}; the strength of the cracked plane f_{fi}; and the crack width at which this occurred w_{ffi}. For specimens MS4 through MS6 no result for f_{ctp} is reported as it was not observed to be distinct from f_{fi}.

Table 1. Monotonic series.

Specimen	A_{cr-pl} (mm^2)	E_c (GPa)	f_{ctsp} (MPa)	f_{fi} (MPa)	w_{ffi} (mm)
MS1	6059	44.9	7.08	7.16	0.479
MS2	6292	44.9	7.53	7.18	0.272
MS3	6181	44.9	5.85	7.46	0.429
MS4	6142	47.2	-	8.67	0.259
MS5	6191	47.2	-	9.32	0.284
MS6	6166	47.2	-	10.40	0.236

Thirty three fatigue tests were also performed and these are listed in Table 2. In the first column: CF refers to specimens that were cycled to failure, that is a cyclic load was applied until the peak of the cyclic load could no longer be resisted by the specimen; and LF refers to specimens that were subjected to a block of cyclic loads N_{blk} and then loaded to failure to determine the effect the cyclic loads had on the monotonic strengths.

Table 2. Fatigue series.

Specimen	A_{cr-pl} (mm^2)	E_c (GPa)	f_{ctsp} (MPa)	f_{fi} (MPa)	w_{ffi} (mm)	T (σ_{tr}/f_{fi})	P (σ_{pk}/f_{fi})	M (σ_m/f_{fi})	R (σ_r/f_{fi})	σ_R (MPa)	σ_m (MPa)
CF-80-S1	6650	47.2	6.34	8.37	0.181	0.089	0.899	0.405	0.810	6.78	3.39
CF-80-S2	6472	47.2	6.66	8.51	0.133	0.091	0.915	0.412	0.824	7.01	3.51
CF-80-S3	6547	47.2	6.34	7.19	0.193	0.090	0.919	0.415	0.829	5.96	2.98
CF-70-S1	6220	44.9	7.26	7.23	0.231	0.083	0.815	0.366	0.731	5.29	2.65
CF-70-S2	6127	44.9	7.36	7.19	0.341	0.083	0.815	0.366	0.733	5.26	2.63
CF-70-S3	6289	44.9	7.76	7.07	0.374	0.078	0.809	0.366	0.732	5.17	2.58
CF-70-S4	6291	47.2	7.24	8.18	0.205	0.081	0.824	0.372	0.743	6.08	3.04
CF-70-S5	6707	47.2	6.95	7.91	0.206	0.084	0.824	0.370	0.739	5.85	2.93
CF-70-S6	6416	47.2	5.58	7.69	0.198	0.085	0.812	0.364	0.727	5.59	2.80
CF-60-S1	6730	47.2	5.25	6.54	0.148	0.085	0.712	0.314	0.627	4.10	2.05
CF-60-S2	6837	47.2	4.83	7.04	0.156	0.086	0.713	0.314	0.628	4.41	2.21
CF-50-S1	6300	44.9	7.46	7.39	0.264	0.087	0.607	0.260	0.520	3.84	1.92
CF-50-S2	6351	44.9	7.76	7.24	0.357	0.085	0.611	0.263	0.526	3.81	1.90
CF-50-S3	6623	44.9	7.17	7.15	0.449	0.089	0.609	0.260	0.521	3.72	1.86
CF-50-S4	6724	44.9	7.23	6.09	0.264	0.087	0.607	0.260	0.520	3.17	1.58
CF-50-S5	6416	47.2	8.09	8.96	0.209	0.088	0.611	0.262	0.523	4.69	2.34
LF-50-S1	6160	44.9	6.66	7.51	0.313	0.086	0.610	0.262	0.525	3.94	1.97
LF-50-S2	6413	44.9	5.74	7.16	0.205	0.084	0.605	0.261	0.520	3.73	1.87
LF-50-S3	6227	44.9	5.93	6.07	0.460	0.085	0.605	0.260	0.520	3.16	1.58
LF-50-S4	6250	44.9	6.20	7.99	0.276	0.085	0.609	0.262	0.524	4.19	2.09
LF-50-S5	6232	44.9	7.67	7.99	0.139	0.085	0.609	0.262	0.523	4.19	2.09
LF-50-S6	6049	44.9	6.05	5.84	0.259	0.085	0.600	0.258	0.515	3.01	1.50
LF-50-S7	6639	44.9	7.42	7.45	0.225	0.085	0.612	0.264	0.527	3.93	1.96
LF-50-S8	5988	44.9	7.43	8.23	0.267	0.086	0.609	0.262	0.523	4.30	2.15
LF-50-S9	6389	44.9	6.65	7.02	0.152	0.086	0.606	0.260	0.520	3.65	1.83
LF-50-S10	6286	44.9	7.22	8.21	0.342	0.085	0.607	0.261	0.523	4.29	2.14
LF-50-S11	6344	47.2	6.10	6.92	0.151	0.093	0.623	0.265	0.530	3.67	1.83
LF-50-S12	6511	44.9	7.70	7.78	0.213	0.084	0.598	0.257	0.514	4.00	2.00
LF-50-S13	6021	44.9	6.27	7.45	0.170	0.085	0.610	0.263	0.524	3.91	1.96
LF-50-S14	6336	44.9	5.49	6.82	0.187	0.085	0.608	0.262	0.523	3.57	1.78
LF-30-S1	6244	44.9	6.22	6.55	0.408	0.091	0.403	0.156	0.311	2.04	1.02
LF-30-S2	6321	44.9	6.65	7.24	0.159	0.491	0.800	0.155	0.309	2.24	1.12
LF-30-S3	6727	44.9	7.49	7.51	0.157	0.089	0.401	0.156	0.312	2.34	1.17

The properties of fibre concrete at a crack depend on the volume, orientation and embedment of the fibre which can vary considerable across the surface of a crack. The maximum strength across the crack plane f_{fi} is a measure of the resistance of the fibres by themselves and consequently allows for the volume, orientation and embedment. For example, if the volume were doubled and somehow the distribution of orientation and embedment maintained then it would be expected that f_{fi} would double. To help reduce the effect of these variables, the fatigue tests were cycled as a proportion of the fibre stress f_{fi} to try to ensure that the fibres were in effect equally stressed. In the first column in Table 2, the two digit number is the range of the cyclic stress as a proportion of f_{fi} given as a percentage. It can be seen that the specimens were grouped in cyclic ranges from 30% to 80% of f_{fi}.

The actual cyclic range applied could only be determined after a test when the area of the cracked plane $A_{cr\text{-}pl}$ could be measured. This is given in Table 2 as R where the cyclic range of the applied stress σ_r is given as a proportion of f_{fi} that is σ_r/f_{fi}. The stress at the trough of a cycle σ_{tr} as a proportion of f_{fi} is shown as T and that at the peak of the cyclic load σ_{pk} as P which are also given as a proportion of f_{fi}. Further, the stress at the mid-cycle σ_m normalised by f_{fi} is shown as M. It can be seen in the T column that the trough of the cyclic load was maintained close to 10% of f_{fi} except for specimen LF-30-S2 where it was increased to 50% to determine the effect of the peak load. Also included in Table 2 for ease of comparison with existing test results is the non-normalised mean stress σ_m and the non-normalised stress range σ_R.

Monotonic test results

The results of the six monotonic tests are shown in Fig. 5(a) where σ is the average stress across the cracked plane and w is the average crack width. The trends are the same in all six tests. Take for example Specimen MS6 which is the upper variation. After cracking, the axial stress increases to the peak value $f_{fi\text{-}MS6}$ at a crack width $w_{ffi\text{-}MS6}$ which is the origin or start of the descending branch. From this origin, there is an almost linear descending branch. Note that the step change at the end of the descending branch is not a material property but is due to a transducer reaching its limit.

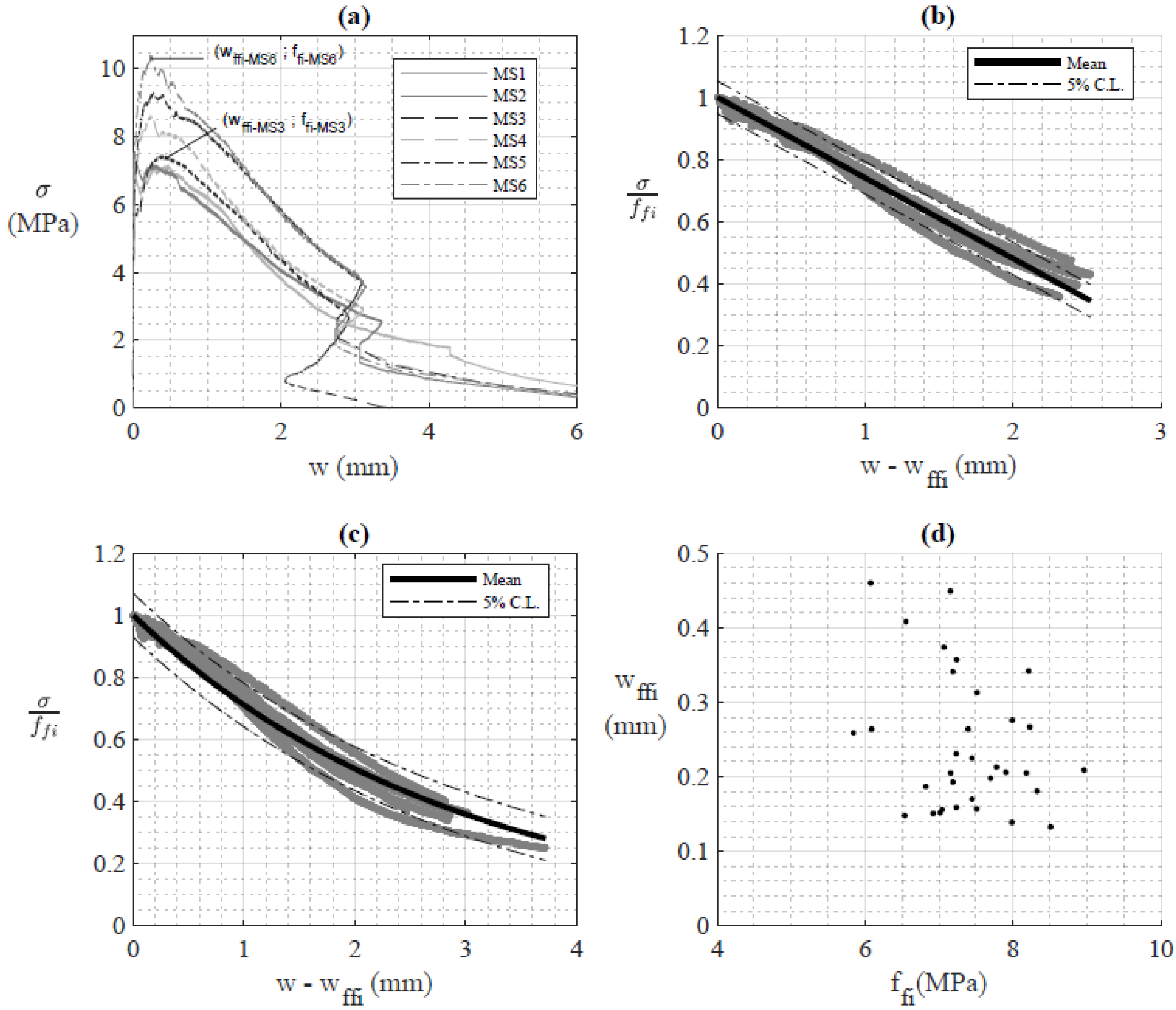

Fig. 5 (a) average crack widths in monotonic tests (b) binear regression of monotonic descending branch, (c) non-linear regression of descending branch, (d) crack width prior to cycling w_{ffi}

So that the origins of all of the descending branches in Fig. 5(a) coincide, the ordinate has been non-dimensionalised by dividing the stresses by f_{fi} for that particular specimen, and the abscissa has been adjusted by subtracting w_{ffi} for that particular specimen, as shown in Fig. 5(b). A linear regression analysis of the monotonic descending branches gives

$$\left(\frac{\sigma}{f_{fi}}\right)_{des-lin} = 1.00 - 0.259(w - w_{ffi}) \qquad (1)$$

in which the crack widths are in mm and which has a standard deviation of

$$SD_{des-lin} = 0.0318 \qquad (2)$$

Similarly, a non-linear regression analysis in Fig. 5(c) gives

$$\left(\frac{\sigma}{f_{fi}}\right)_{des-non} = e^{-0.341(w-w_{ffi})} \qquad (3)$$

for which the standard deviation is

$$SD_{des-non} = 0.0428 \qquad (4)$$

and which is larger than that from the linear regression in Eq. 2, however, the non-linear regression has a better fit towards the end of the descending branch.

All of the fatigue tests were loaded monotonically prior to cyclic loading so f_{fi} and w_{ffi} were also measured and are listed in Table 2. All of the values of w_{ffi} in Tables 1 and 2 are plotted in Fig. 5(d) which has a mean value of

$$w_{ffi} = 0.242\,mm \qquad (5)$$

and a standard deviation of

$$SD_{wffi} = 0.0916 \qquad (6)$$

It can be seen in Fig. 5(d) that w_{ffi} has no correlation with f_{fi} which would suggest the equivalent stresses in the fibres are the same and therefore the crack width does not increase with f_{fi}. This further suggests that the parameter σ/f_{fi} is a useful tool in reducing the scatter. An example of a crack face after testing is shown in Fig. 6.

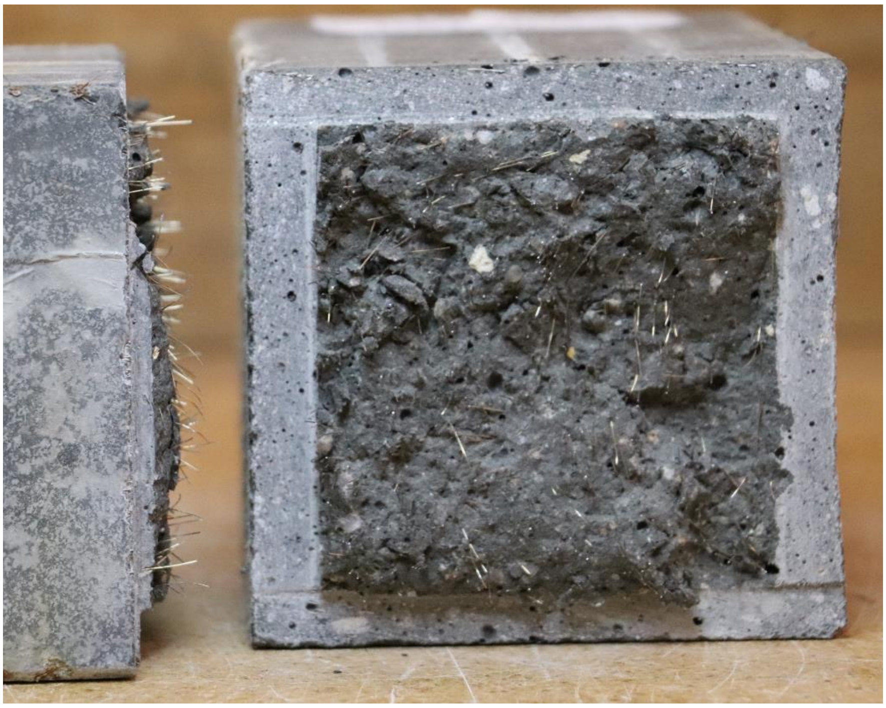

Fig. 6 Specimen LF-30-S1 after testing

General behaviour of fatigue tests

The results of testing Specimen CF-80-S3 are shown in Fig. 7(a). The specimen was first loaded to its peak strength of f_{fi} that is at $\sigma/f_{fi} = 1$ at Point A. A cyclic load was then applied with a range of $0.8f_{fi}$ that had a peak of $0.9f_{fi}$ and a trough of $0.1f_{fi}$ as shown. The cyclic load caused an increase in crack width and the specimen was cycled to failure. Initially the cyclic peak was maintained at $0.9f_{fi}$ but towards the end of the test the peak load could not be maintained and reduced. Also plotted in Fig. 7(a) is the monotonic descending branch and the 5% confidence limits from Eqs. 1 and 2 and the monotonic non-linear variation from Eq. 3. It can be seen that the cyclic data converges onto the monotonic descending branch.

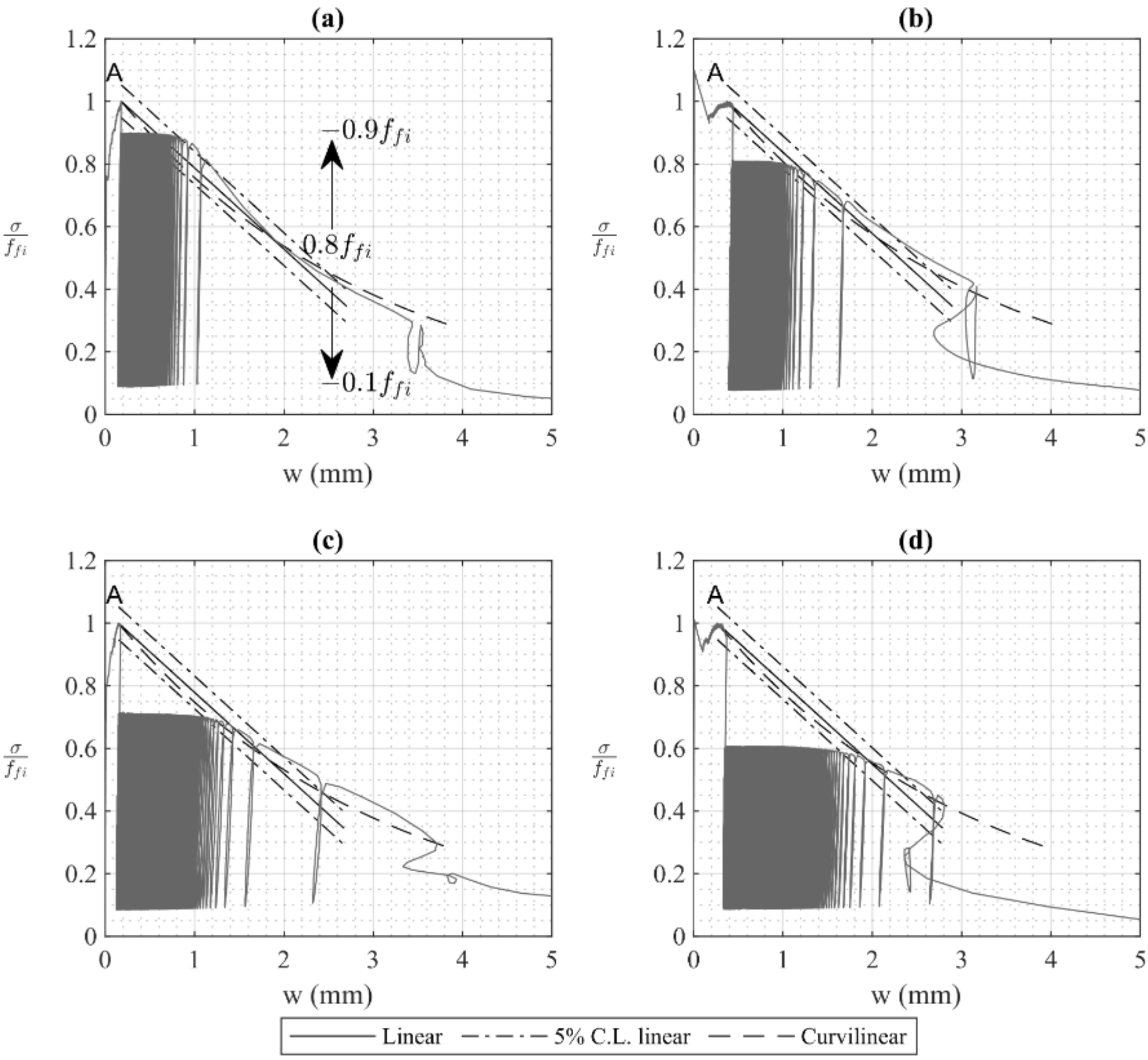

Fig. 7 Cycled to failure at: (a) 80% range, (b) 70% range, (c) 60% range, (d) 50% range

Specimen CF-70-S3 in Fig. 7(b) was cycled at a range of $0.7f_{fi}$ that is at 70% of f_{fi}, CF-60-S1 in Fig. 7(c) at $0.6f_{fi}$ and CF-50-S1 in Fig. 7(d) at $0.5f_{fi}$ and they all also converge to the monotonic variation.

Specimen LF-50-S3 in Fig. 8(a) was subjected to a block of cyclic loads at a range of $0.5f_{fi}$ and then loaded to failure. In Fig. 8(b), specimen LF-30-S1, a block at a range of $0.3f_{fi}$ was applied and then loaded to failure. It can be seen that on loading to failure the experimental data also converged on to the monotonic variation.

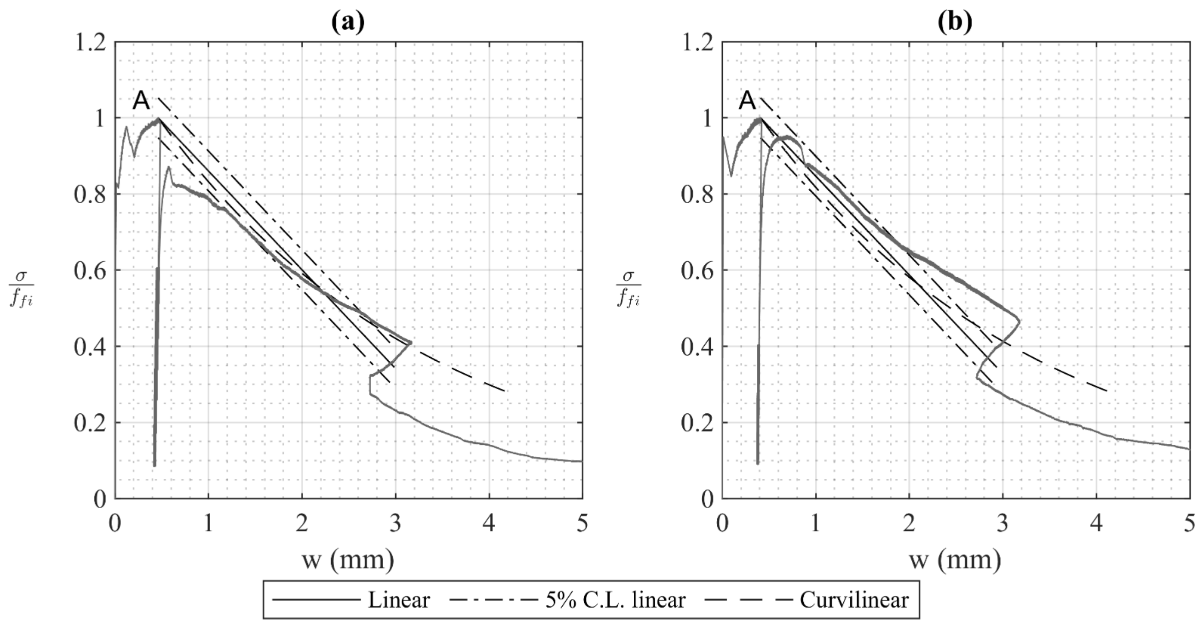

Fig. 8(a) cycled at 50% range then loaded to failure, (b) cycled at 30% range with peak at 40% then loaded to failure

Whether the specimen was cycled to failure or loaded to failure, all the data converged onto the monotonic variation. This occurred in all of the tests which are given in the supplementary material Figs. S1-S7. The monotonic descending branches in Fig. 5(a) and (b) are caused by a gradual debonding of the fibres. The fact that after cyclic loading all of the test data then converged onto the monotonic variation shows that all of the cyclic behaviour is governed by debonding. Hence if the effect of cyclic loading on the crack width can be predicted, which is the subject of the next section, then the fatigue damage due to cyclic loading can also be predicted.

From the above cyclic tests, the behaviour under cyclic loading can be idealised as in Fig. 9 which also introduces new nomenclature to help in the description and in the ensuing quantification. Under displacement control, cracking starts at f_{ctsp} at Point A causing a reduction of the stress as the fibres take up the load. The stress then increases until the fibres reach their maximum resistance of f_{fi} at Point B where the crack width is w_{ffi}. Unloading would occur at a stiffness $k_{st\text{-}cy}$. A cyclic range of stress σ_r is then applied in at a peak stress σ_{pk} and trough σ_{tr}. The increase in the crack width due to one cycle of load is $dw/dN = \beta$ which is the incremental set. The analysis in the following section shows that there is at first a stable or constant incremental set β_{stb} over the first E_{stb} cycles. At the end of the E_{stb} cycles, shown as Point E, the crack width is w_{stb} and the cyclic stiffness k_{stb}. After this stable region, there is then an unstable region in which there is a rapid increase in the incremental set. Point F is when σ_{pk} has reduced by 1% and is used as a measure of the end of the unstable region as, beyond which, the increase in crack width is so large the specimen in effect fails monotonically. At Point F, the number of cycles is $E_{1\%}$, the crack width $w_{1\%}$ and the cyclic stiffness $k_{1\%}$. The incremental set in the unstable region from Point E to Point F continually increases with cycles. The average incremental set in this unstable region β_{unstb} can be derived directly from Points E and F. The residual strength of the specimen has reduced to σ_{pk} at Point F. Alternatively, after a block of N_{blk} cycles at Point C, should the specimen be loaded to failure then Point D is the residual strength $f_{fi\text{-}cy}$ at a crack width after cycling of $w_{ffi\text{-}cy}$.

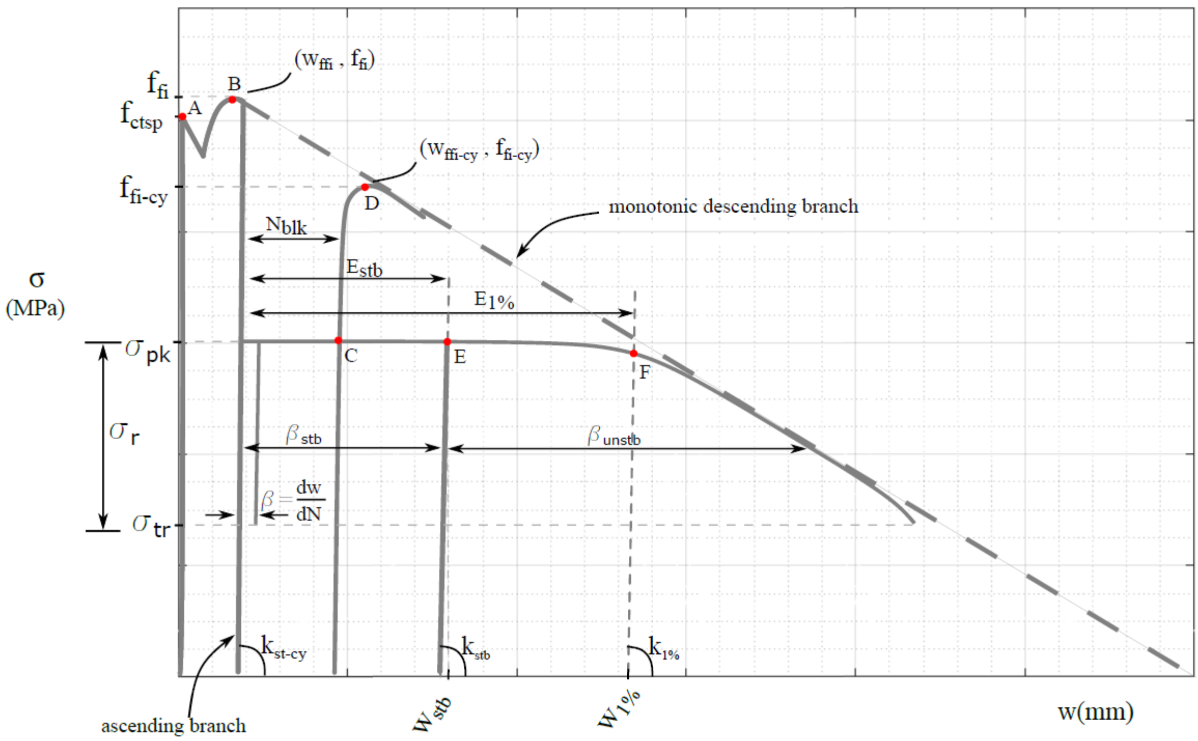

Fig. 9 Parameters that govern cyclic behaviour

From the cyclic tests cycled to failure in the supplementary material Figs. S1-S7, E_{stb} and w_{stb} and $E_{1\%}$ and $w_{1\%}$ are listed in Table 3. From the cyclic tests loaded to failure in Figs. S1-S7, f_{fi-cy}, w_{ffi-cy}, the number of cycles in the applied block N_{blk}, and the crack width at the end of the block w_{Nblk} are listed in Table 4.

Table 3. Results from fatigue specimens cycled to failure.

Specimen	E_{stb}	w_{stb} (mm)	$E_{1\%}$	$w_{1\%}$ (mm)	$E_{1\%}$ / E_{stb}
CF-80-S1	380	0.313	581	0.804	1.529
CF-80-S2	550	0.322	840	1.004	1.527
CF-80-S3	120*	0.487	123*	0.549	1.025
CF-70-S1	80	0.427	134	0.815	1.675
CF-70-S2	3500	0.521	4308	1.063	1.231
CF-70-S3	525	0.455	1314	1.010	2.503
CF-70-S4	19500	0.400	21440	1.303	1.099
CF-70-S5	1900	0.370	2637	1.054	1.388
CF-70-S6	41000	0.281	46052	1.152	1.123
CF-60-S1	110000	0.149	153908	1.057	1.399
CF-60-S2	160000	0.173	203811	0.929	1.274
CF-50-S1	1820000	0.358	2432852	1.330	1.337
CF-50-S2	900000	0.393	1374622	1.153	1.527
CF-50-S3	180000	0.464	218344	1.127	1.213
CF-50-S4	410000	0.342	465852	1.017	1.136
CF-50-S5	600000	0.277	718776	1.095	1.198

*outlier omitted from analyses

Table 4. Results from fatigue specimens loaded to failure.

Specimen	$f_{fi\text{-}cy}$ (MPa)	$w_{fi\text{-}cy}$ (mm)	w_{Nblk} (mm)	N_{blk}
LF-50-S1	7.577	0.427	0.282	6845190
LF-50-S2	7.594	0.388	0.210	6552613
LF-50-S3	5.298	0.571	0.450	6851115
LF-50-S4	8.030	0.518	0.273	404946
LF-50-S5	7.439	0.240	0.139	405001
LF-50-S6	5.574	0.368	0.250	405005
LF-50-S7	7.035	0.434	0.252	811046
LF-50-S8	7.836	0.401	0.256	729604
LF-50-S9	7.206	0.506	0.165	810001
LF-50-S10	6.858	0.580	0.344	1215018
LF-50-S11	7.035	0.294	0.166	1214951
LF-50-S12	6.536	0.299	0.239	1620001
LF-50-S13	6.824	0.441	0.206	1620001
LF-50-S14	6.801	0.454	0.213	1619951
LF-30-S1	6.240	0.714	-	6189803
LF-30-S2	7.815	0.412	-	6543022
LF-30-S3	7.536	0.385	0.141	2620841

For the specimens loaded to failure in Table 4, the residual strength $f_{fi\text{-}cy}/f_{fi}$ and the increase in crack width at which this occurred $w_{ffi\text{-}cy}$-w_{ffi} is plotted as a circle in Fig. 10 where it can be seen that they are clustered about the monotonic strength from Eq. 1. For the specimens cycled to failure in Table 3, the residual strength at $E_{1\%}$ that is σ_{pk}/f_{fi} at the increase in crack width $w_{1\%}$-w_{ffi} is plotted as a positive sign and these are also clustered about the monotonic from Eq. 1. This is further confirmation that monotonic descending branch governs the behaviour.

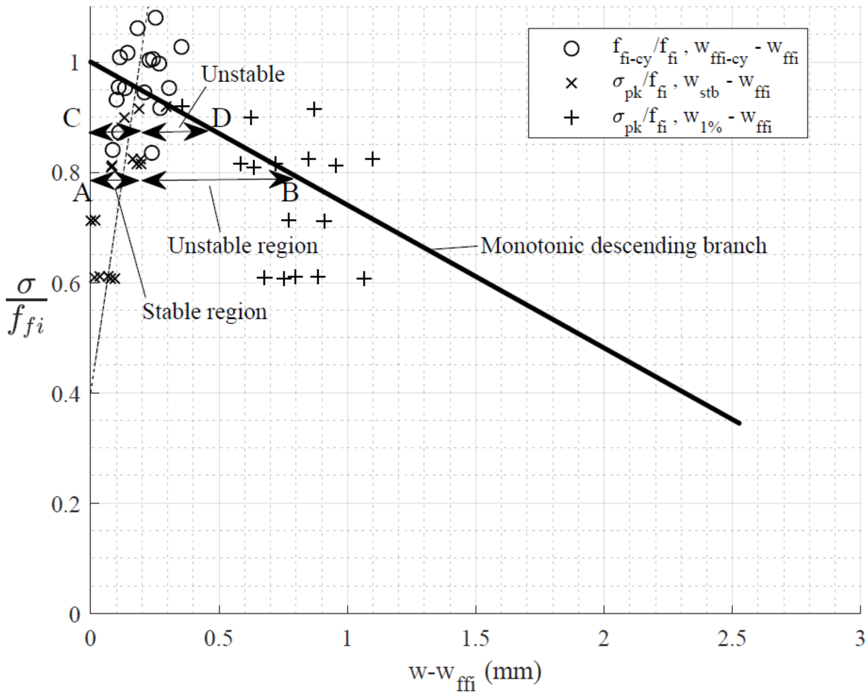

Fig. 10 Residual strengths

Incremental set data

Specimen CF-80-S1 was cycled to failure with a range of $0.8f_{fi}$. From the data from the tension test described above, the variation of the total crack width w with the number of cycles is shown in Fig. 11(a). The initial part A-B can be seen to be linear with a constant slope of β_{stb} up to E_{stb} cycles when the crack width is w_{stb}. This means that each cycle of load caused the same increase in crack width, that is the system is stable. Beyond this stable region, the slope increases rapidly such that subsequent cycles cause increasing changes in crack width; this will be referred to as the unstable region. An average incremental set for this unstable region β_{unstb}

can be derived from the slope between the coordinate (E_{stb}, w_{stb}) in Fig. 11(a) and ($E_{1\%}$, $w_{1\%}$) from Table 3.

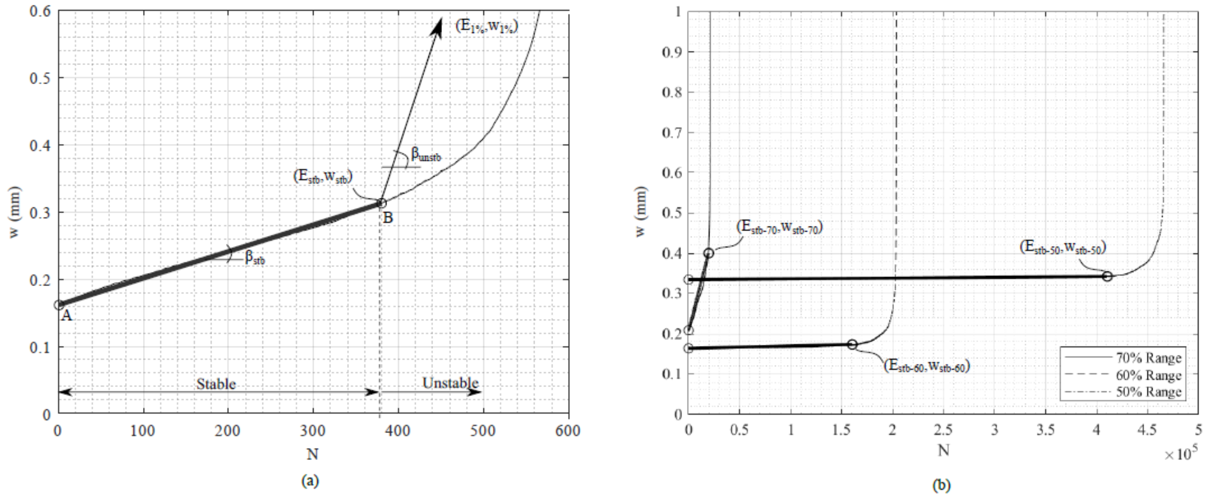

Fig. 11(a) CF-80-S1 Variation in crack width – range 80%, (b) variation in crack width for ranges 70% , 60% and 50%

Further examples at decreasing ranges are shown in Fig. 11(b). As the range reduces the endurance increases but the shape consisting of the stable and unstable regions remains the same.

The analyses for all of the specimens are given in the supplementary material Figs. S8-14. They can be idealised as in Fig. 12. Initially the crack width can reduce very slightly from A to B which, it is felt, is more due to the settling down of the rig than a material property. It can remain horizontal as in A-C such that there is no increase in crack width and, therefore, no damage. Or it can increase along A-D where each cycle of load causes the same increase in crack width, that is a stable incremental set. Whether the path follows A-B-D, A-C-D or A-D, the stable incremental set β_{stb} was measured as shown that is from A to D. Beyond D, the incremental set increases rapidly and with each cycle. This is quantified using the average incremental set in this unstable region β_{unstb} by taking the average value that is the slope of the linear variation from the coordinates (E_{stb}, w_{stb}) to ($E_{1\%}$, $w_{1\%}$) as shown.

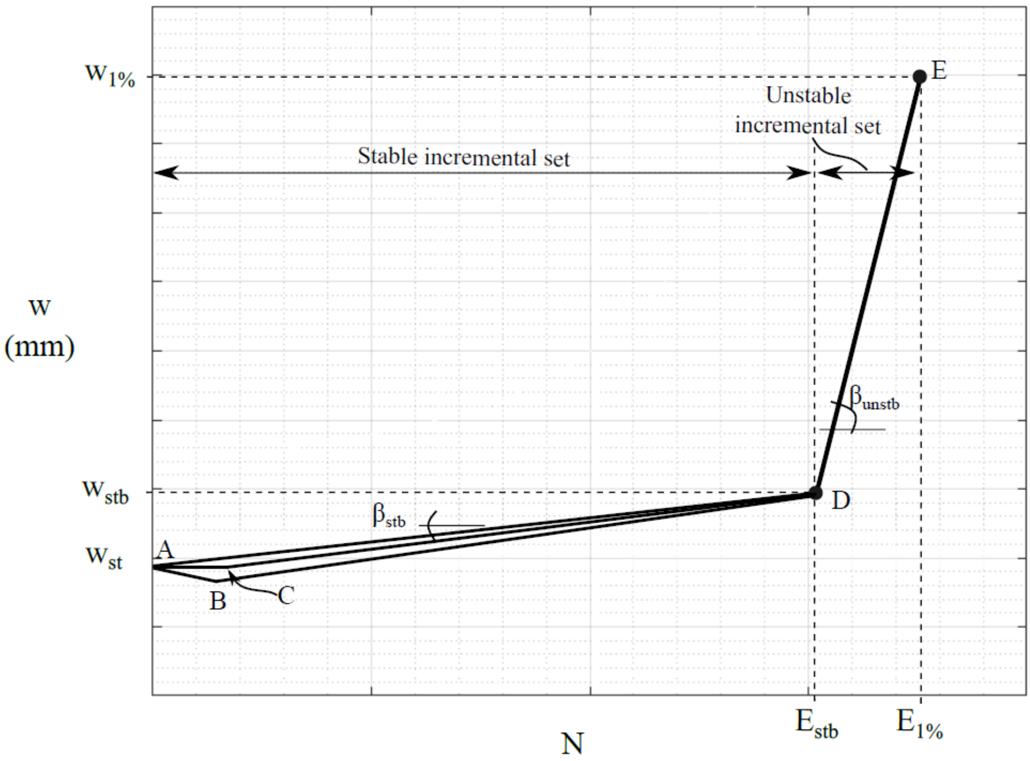

Fig. 12 Idealised stable and unstable regions

The stable increment set β_{stb} can be extracted from all the analyses of all the specimens in the supplementary material Figs. S8-14 as it only requires the slope and the results are given in Table 5. The limits to β_{stb}, that is E_{stb} and w_{stb}, can only be extracted from the specimens that cycled to failure and their values are listed in Table 3. As explained previously, the unstable incremental set β_{unstb} can be derived from the endurances and crack widths in Table 3 and their values are listed in Table 5.

Table 5. Results of incremental set analyses.

Specimen	β_{unstb}	β_{stb}	β_{stb_mn}
CF-80-S1	2.447E-03	3.980E-04	
CF-80-S2	2.352E-03	3.453E-04	1.05E-03
CF-80-S3	2.052E-02	2.399E-03	
CF-70-S1	7.174E-03	1.157E-03*	-
CF-70-S2	6.703E-04	4.212E-05	
CF-70-S3	7.034E-04	6.694E-05	
CF-70-S4	4.653E-04	9.814E-06	3.81E-05
CF-70-S5	9.277E-04	6.955E-05	
CF-70-S6	1.724E-04	2.063E-06	
CF-60-S1	2.069E-05	5.967E-08	6.03E-08
CF-60-S2	1.724E-05	6.092E-08	
CF-50-S1	1.587E-06	6.273E-09	
CF-50-S2	1.602E-06	1.426E-08	
CF-50-S3	1.727E-05	3.177E-08	
CF-50-S4	1.209E-05	1.875E-08	
CF-50-S5	6.881E-06	2.404E-08	
LF-50-S1	-	-2.751E-11	
LF-50-S2	-	-9.142E-11	
LF-50-S3	-	2.113E-09	
LF-50-S4	-	3.847E-09	
LF-50-S5	-	7.337E-09	7.20E-09
LF-50-S6	-	3.215E-09	
LF-50-S7	-	3.402E-09	
LF-50-S8	-	2.862E-09	
LF-50-S9	-	4.160E-09	
LF-50-S10	-	4.256E-09	
LF-50-S11	-	2.382E-09	
LF-50-S12	-	3.326E-09	
LF-50-S13	-	4.194E-09	
LF-50-S14	-	8.129E-10	
LF-30-S1	-	1.410E-10	
LF-30-S2	-	9.090E-10	1.061E-10
LF-30-S3	-	-7.318E-10	

*outlier omitted from analyses

Now let us consider possible outliers in the β values in Table 5. As we are dealing with fatigue, such that the log of the variable matters, a single order of magnitude variation does not suggest an outlier. In the β_{unstb} column, the values of β_{unstb} within each group of a specific range do not vary by more than an order of magnitude so there does not appear to be any outliers.

In the β_{stb} column in Table 5 and starting with the $0.8f_{fi}$ range, the values only vary by one order of magnitude so there are no outliers; the mean of 1.05E-3 is shown in the column labelled β_{stb-mn}. In the following $0.70f_{fi}$ range, specimen CF-70-S1 is two orders of magnitude larger than the average of the remaining samples which suggests that this β_{stb} is an outlier and as such has been marked with an asterisk and will not be used in the ensuing statistical analyses. The mean of the remainder is 3.81E-5 as shown. There is no outlier in the $0.60f_{fi}$ range. In the $0.50f_{fi}$ range, except for LF-50-S1 and LF-50-S2 where there was no measurable incremental set, all are close. As these incremental sets are miniscule, it is felt that LF-50-S1 and LF-50-S2 are part of this population. Finally for the $0.30f_{fi}$ range, the incremental sets are even smaller and can be considered zero.

The comparison of $E_{1\%}$ to E_{stb} in Table 3, that is $E_{1\%}/E_{stb}$, shows that on average the increase in endurance from E_{stb} to $E_{1\%}$ is one-third of E_{stb}. That is, unstable crack propagation is associated only with one-quarter of the total number of cycles than can be applied. Specimen CF-80-S3 is the only exception as the increase is only 3% and, hence, it will be considered as an outlier such that E_{stb} and $E_{1\%}$ will not be used in the following statistical analyses.

The crack widths at the end of the stable incremental set that is w_{stb} in Table 3 have been plotted in Fig. 10 as the coordinates (σ_{pk}/f_{fi}, w_{stb}-w_{ffi}) shown as a cross (x) and a dashed line has been drawn through the mean. It can be seen, such as along A-B, that the unstable region is in general much larger than the stable region even though only one-quarter of the number of cycles occur in this region. It is also worth noting that as the peak load is increased such as along C-D, the allowable width of crack in the unstable region diminishes; this limits the number of cycles that can be applied before a reduction in load along the monotonic descending branch.

In most fatigue analyses, such as those with stud shear connectors that also exhibit an incremental set (Oehlers and Bradford 1995), the range of load as opposed to the peak load is the main parameter that governs the fatigue damage. Because of this, no attempt was made to vary the peak load independently of the range except for Specimen LF-30-S2 where the range was $0.30f_{fi}$ and the peak load was increased to $0.80f_{fi}$ in comparison to Specimen LF-30-S1 which had the same range of $0.30f_{fi}$ but a peak load of $0.40f_{fi}$. If the peak load was the major parameter that governed fatigue damage, then specimen LF-30-S2 would behave like the specimens in the group CF-70 where $\beta_{stb\text{-}mn}$ in Table 5 is 3.81E-05. Specimen LF-30-S2 has a β_{stb} value of 9.09E-10 which is five orders of magnitude smaller and much closer to the other two specimens at $0.30f_{fi}$ which had a mean value of 2.95E-10, that is virtually no incremental set. Hence it is clear that the peak load does not govern the fatigue damage, that is the incremental set, to anywhere near the same extent as the range. However as can be seen in Fig. 10, increasing the peak load does reduce the allowable crack widening and through this procedure reduces the allowable number of cycles.

Linear regression analysis of incremental set data

Linear analysis of stable incremental set $\beta_{stb\text{-}lin}$

The incremental sets β_{stb} in Table 5 are plotted in Fig. 13(a). It can be seen that a linear variation through all the points is not suitable. However, it does seem reasonable for all the results excluding the 30% range. Also excluded from the analyses are the two negative values of β_{stb}

for Specimens LF-50-S1 and LF-50-S2 which in reality are zero values as these cannot be input into a log scale; this omission will produce a slightly conservative result.

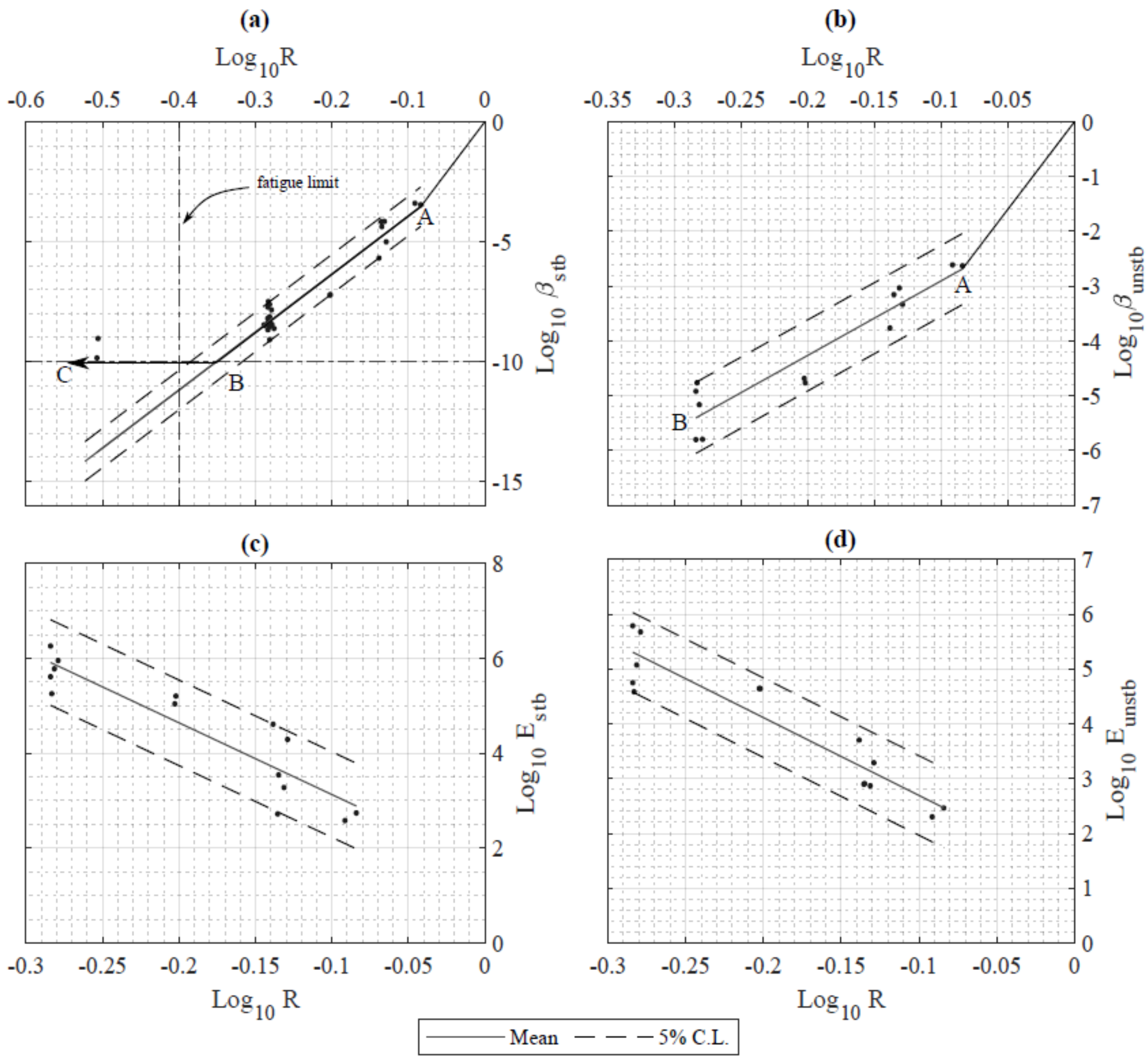

Fig. 13(a) Stable incremental set β_{stb} , (b) Unstable incremental set β_{unstb}, (c) stable endurance E_{stb}, (d) unstable endurance E_{unstb}

A linear regression analysis of $\log_{10}\beta_{stb}$ (excluding both the outlier, the negative values and the results from the 30% range) in Fig. 13(a) gave

$$log_{10}\beta_{stb-lin} = -1.514 + 24.19log_{10}R \qquad (7)$$

where R is the cyclic range of stress as a proportion of f_{fi}, that is σ_r/f_{fi}, and in which the standard deviation is

$$SD_{\beta stb-lin} = 0.499 \tag{8}$$

It can be seen in Table 5 that the 30% range has a been value of $\beta_{stb\text{-}mn}$ of 1.061E-10 which is very closed to E-10. Hence it is suggested that E-10 be used as a bound to the variation in Eq. 7, that is

$$log_{10}\beta_{stb-lin} \geq -10 \tag{9}$$

such that the bi-linear variation A-B-C in Fig. 13(a) defines the incremental set. Furthermore for convenience of analysis at large ranges, O-A through the origin can be used where A is at the 80% range such that O-A is given by

$$log_{10}\beta_{stb-lin} = 39.81 log_{10}R \tag{10}$$

From Eqs. 7 and 9, the transition between these lines occurs at a range

$$R_{tran} = 0.446 \tag{11}$$

Equations 7 and 8 can be written as

$$\beta_{stb-lin} = 0.0306R^{24.2}10^{\pm xSD_{\beta stb-lin}} \tag{12}$$

where *x* is the number of standard deviations to achieve the required confidence limit and where a positive value of *x* will achieve the larger incremental set.

Hence in the stable region and when a block of N_{blk} cycles is applied, then from Eq. 12 the increase, based on the linear variation, in crack width is given by

$$\Delta w_{stb-lin} = N_{blk}0.0306R^{24.2}10^{\pm xSD_{\beta stb-lin}} \tag{13}$$

Linear analysis of mean of stable incremental set $\beta_{stb-mn-lin}$

A linear analysis of the means β_{stb-mn} in Table 5 weighted with respect to the number of specimens in a specific range gave

$$\beta_{stb-mn-lin} = 0.0879R^{25.3}10^{\pm xSD_{\beta stb-lin}} \tag{14}$$

It is felt that this will give a less conservative prediction of the incremental set, as it allows for the negative values which were omitted in deriving Eq. 12 as they could not be included in the log analysis. As can be seen in Eq. 14, it is suggested that Eq. 8 be used for the standard deviation.

Linear analysis of unstable incremental set $\beta_{unstb-lin}$

Applying the above approach to the β_{unstb} values in Table 5, the log analysis shown in Fig. 13(b) from A to B gives

$$log_{10}\beta_{unstb-lin} = -1.545 + 13.58log_{10}R \qquad (15)$$

with a standard deviation of

$$SD_{\beta unstb-lin} = 0.394 \qquad (16)$$

which gives

$$\beta_{unstb-lin} = 0.0285R^{13.6}10^{\pm xSD_{\beta unstb-lin}} \qquad (17)$$

Furthermore and for ranges greater than 80%, O-A is given by

$$log_{10}\beta_{unstb-lin} = 29.52log_{10}R \qquad (18)$$

Hence in the unstable region and when a block of N_{blk} cycles is applied, then using Eq. 17, the increase in crack width is given by

$$\Delta w_{unstb-lin} = N_{blk}0.0285\, R^{13.6}10^{\pm xSD_{\beta unstb-lin}} \qquad (19)$$

Linear analysis of limit to stable endurance $E_{stb-lin}$

The limit to the stable incremental set β_{stb} is E_{stb} and the analysis of these results in Table 3 is shown in Fig. 13(c). The standard deviation of the log of the variable is

$$SD_{Estb-lin} = 0.548 \qquad (20)$$

and the regression is given by

$$E_{stb-lin} = 41.12R^{-15.1}10^{\pm xSD_{Estb-lin}} \qquad (21)$$

Linear analysis of range of unstable endurance $E_{unstbl-lin}$

The number of cycles within the unstable region where β_{unstb} controls is given by E_{unstb} which is equal to $E_{1\%}$-E_{stb} in Table 3. The analysis of these results is shown in Fig. 13(d) in which the standard deviation is

$$SD_{Eunstb-lin} = 0.441 \qquad (22)$$

and the regression is given by

$$E_{unstb-lin} = 18.7R^{-14.2}10^{\pm xSD_{Eunstb-lin}} \qquad (23)$$

The increase in crack width at the transition from the stable incremental set to the unstable incremental set Δw_{tran} is the product of Eqs. 12 and 21 which gives

$$\Delta w_{tran} = 1.258R^{9.1}10^{\pm xSD_{Estb-lin} \pm xSD_{\beta stb-lin}} \qquad (24)$$

Curvilinear analysis of incremental set data

The fatigue data was also analysed using a curvilinear log analysis through the origin. Consider for example Fig. 13(a) where at the origin the anti-log of the range and incremental set is 1. This means that when the cyclic range is equal to the maximum strength f_{fi} then the increase in the crack width over that one cycle is very large at 1mm, that is failure is very rapid which is appropriate. For the endurance such as in Fig. 13(c), at the origin, the range is also equal to the peak strength and the endurance is one cycle which is also appropriate.

Curvilinear analysis of stable incremental set $\beta_{stb\text{-}curv}$

The curvilinear analysis through the origin is shown in Fig. 14(a) where the standard deviation is

$$SD_{\beta stb-curv} = 0.467 \quad (25)$$

and the curvilinear fit is

$$log_{10}(\beta_{stb-curv}) = 47.7(log_{10}R)^2 + 42.9log_{10}R \pm xSD_{\beta stb-curv} \quad (26)$$

which can be written as

$$\beta_{stb-curv} = 10^{47.7(log_{10}R)^2} R^{42.9} 10^{\pm xSD_{\beta stb-curv}} \quad (27)$$

It can be seen that the standard deviation for this curvilinear analysis of 0.467 in Eq. 25 is 6% smaller than that of the linear analysis of 0.499 in Eq. 8 even though the curvilinear analysis has the additional results from the 30% range.

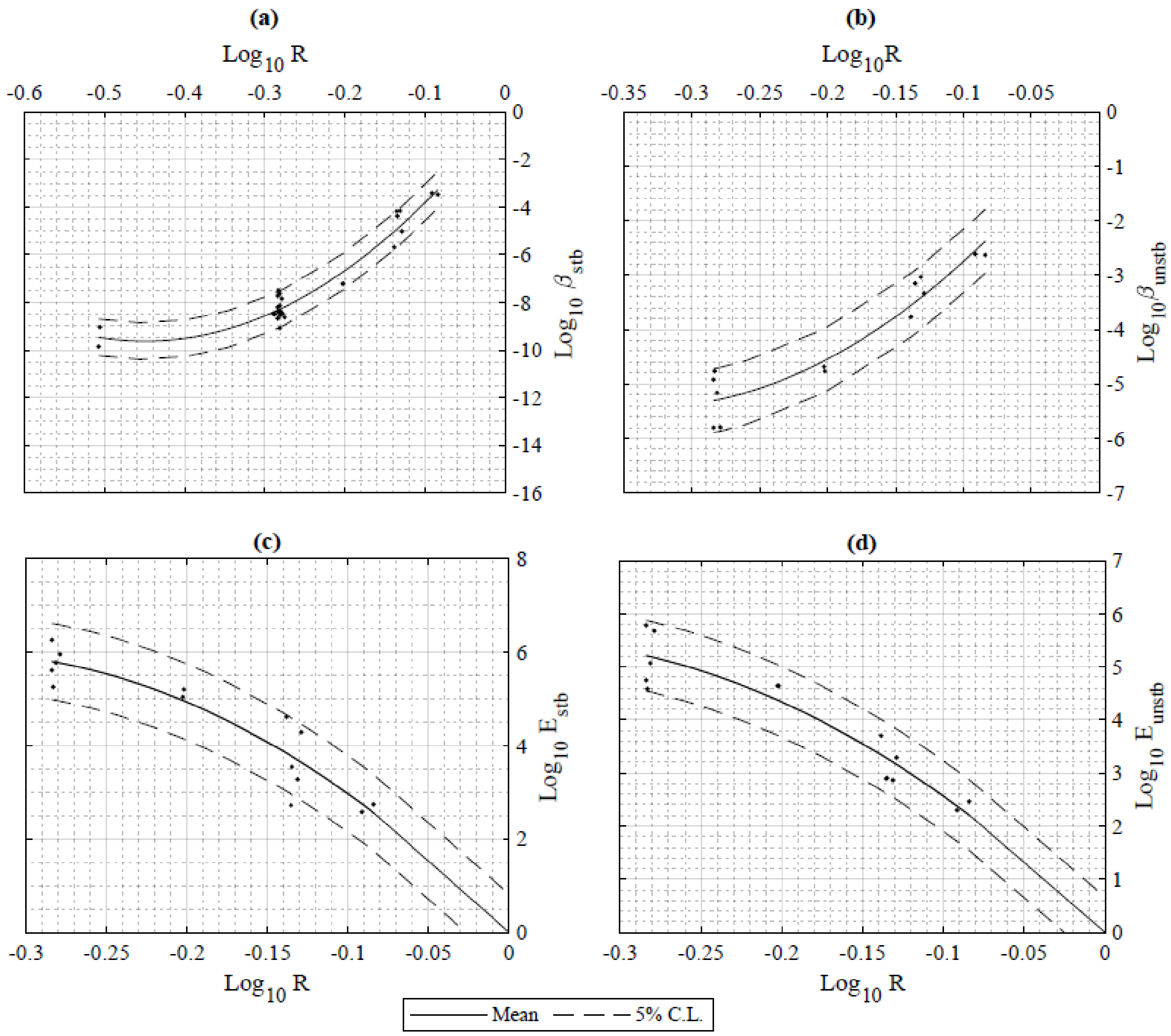

Fig. 14(a) curvilinear analysis of β_{stb} (b) curvilinear analysis of $\beta_{unstb-curv}$, (c) curvilinear analysis of $E_{stb-curv}$, (d) curvilinear analysis E_{unstb}

Curvilinear analysis of mean of stable incremental set $\beta_{stb-mn-curv}$

A curvilinear analysis of β_{stb-mn} in Table 5, with each point weighted in accordance to the number of tests in that range, gave

$$\beta_{stb-mn-curv} = 10^{40.342(log_{10}R)^2} R^{40.6} 10^{\pm xSD_{\beta stb-curv}} \qquad (28)$$

It was felt that this would give a better estimate of the true fit as the means included the negative values, whereas, the fit in Eq. 14(b) excluded these values and, hence, was conservative. It is suggested that the fit in Eq. 28 with the SD in Eq. 25 would give the best estimate the incremental set.

Curvilinear analysis of unstable incremental set $\beta_{unstb\text{-}curv}$

The curvilinear analysis of the unstable incremental set is shown in Fig. 14(b). The standard deviation is

$$SD_{\beta unstb-curv} = 0.356 \qquad (29)$$

which is 10% smaller than that from the linear analysis in Eq. 16. The regression is given by

$$\beta_{unstb-curv} = 10^{47.8(log_{10}R)^2} R^{32.3} 10^{\pm xSD_{\beta unstb-curv}} \qquad (30)$$

Curvilinear analysis of limit to stable endurance $E_{stb\text{-}curv}$

The curvilinear analysis of the stable endurance in Fig. 14(c) has a standard deviation of

$$SD_{Estb-curv} = 0.505 \qquad (31)$$

which is 8% smaller than that from the linear analysis in Eq. 20. The regression is

$$E_{stb-curv} = 10^{-50.2(log_{10}R)^2} R^{-34.7} 10^{\pm xSD_{Estb-curv}} \qquad (32)$$

Curvilinear analysis of range of unstable endurance $E_{unstbl\text{-}curv}$

For the unstable endurance, the results are shown in Fig. 14(d) where the standard deviation is

$$SD_{Eunstb-curv} = 0.405 \qquad (33)$$

which is 8% smaller than in the linear approach in Eq. 22. The regression is given by

$$E_{unstb-curv} = 10^{-39.7(log_{10}R)^2} R^{-29.6} 10^{\pm xSD_{Eunstb-curv}} \qquad (34)$$

It can be seen that the curvilinear analysis as compared to the linear analysis provides a reduction to the scatter.

Cyclic stiffness

A typical variation of the cyclic stiffness during a specimen test is shown in Fig. 15 and the results from all tests are provided in the supplementary material Figs. S15 to S21. At the start of cyclic loading, there is a rapid reduction in stiffness which is felt to be a bedding down of the rig rather than a material property. There is then a gradual reduction in stiffness during the region of stable incremental set up, that is up to E_{stb} where the cyclic stiffness is k_{stb}; after which there is a rapid reduction in stiffness particularly after $E_{1\%}$ where the cyclic stiffness is $k_{1\%}$. The data within the stable region was subjected to a linear regression where the slope is m_k and the intercept with the ordinate was considered to be the best estimate of the cyclic stiffness at the start of cyclic loading $k_{st\text{-}cy}$. The values of these parameters for each test are given in Table 6 with their mean, standard deviation and coefficient of variation.

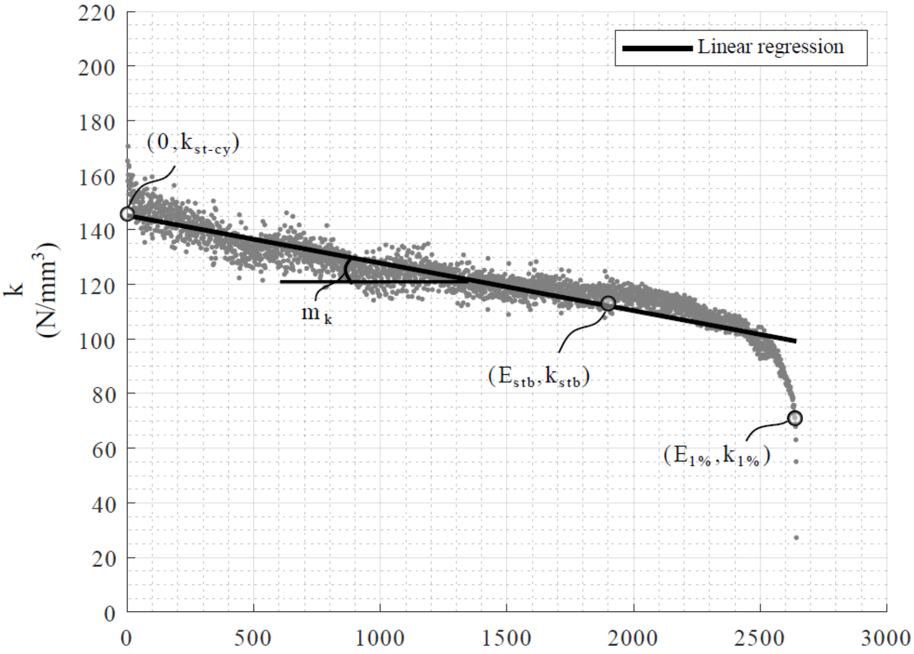

Fig. 15 Variation in cyclic stiffness of CF-70-S5.

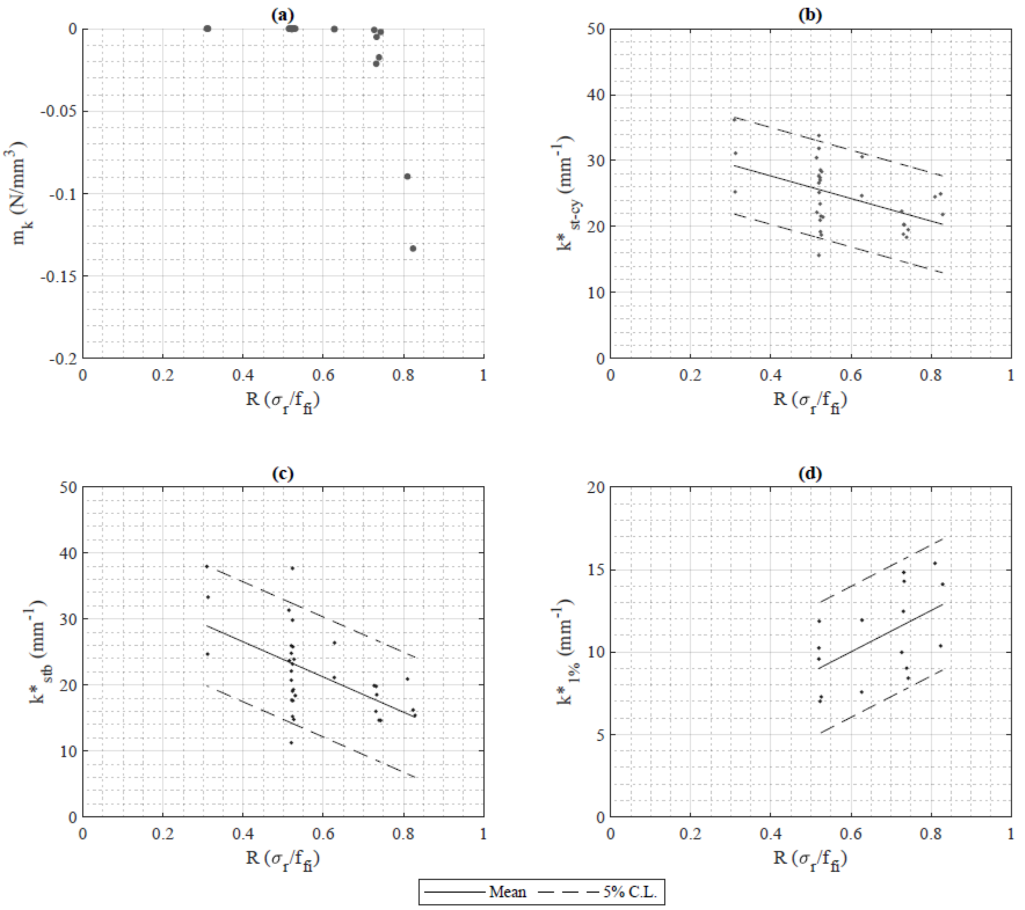

Fig. 16(a) Variation in m_k with R, (b) cyclic stiffness at the start of cyclic loading, (c) cyclic stiffness at E_{stb}, (d) Cyclic stiffness at $E_{1\%}$

Table 6. Cyclic stiffness results.

Specimen	$k_{st\text{-}cy}$ N/mm^3	k_{stb} N/mm^3	$k_{1\%}$ N/mm^3	m_k N/mm^3	$k^*_{st\_cy}$ mm^{-1}	k^*_{stb} mm^{-1}	$k^*_{1\%}$ mm^{-1}
CF-80-S1	204	174	128	-8.96E-02	24.5	20.9	15.4
CF-80-S2	212	138	88.3	-1.33E-01	24.9	16.2	10.4
CF-80-S3	157	111	101	-4.40E-01	21.8	15.4	14.1
CF-70-S1	136	116	90.2	-3.01E-01	18.9	16.0	12.5
CF-70-S2	146	133	103	-5.04E-03	20.3	18.5	14.3
CF-70-S3	144	140	105	-2.13E-02	20.3	19.8	14.8
CF-70-S4	160	120	68.8	-2.08E-03	19.5	14.6	8.41
CF-70-S5	145	116	71.3	-1.74E-02	18.4	14.7	9.02
CF-70-S6	172	153	76.7	-7.93E-04	22.3	19.9	10.0
CF-60-S1	161	138	49.5	-3.21E-04	24.7	21.1	7.57
CF-60-S2	215	186	84.0	-2.92E-04	30.6	26.4	11.9
CF-50-S1	205	153	70.8	-2.91E-05	27.7	20.7	9.58
CF-50-S2	136	107	52.7	-3.65E-05	18.7	14.8	7.28
CF-50-S3	180	127	84.8	-2.52E-04	25.2	17.7	11.9
CF-50-S4	206	135	62.3	-2.03E-04	33.8	22.1	10.2
CF-50-S5	210	136	62.8	-1.27E-04	23.4	15.2	7.01
LF-50-S1	162	145		-2.22E-06	21.6	19.3	
LF-50-S2	190	177		-2.79E-06	26.6	24.8	
LF-50-S3	95	68		-3.84E-06	15.6	11.2	
LF-50-S4	153	141		-1.88E-05	19.2	23.7	
LF-50-S5	371	301		-2.21E-04	46.5*	23.9	
LF-50-S6	129	138		-2.80E-05	22.2	19.1	
LF-50-S7	211	178		-2.81E-05	28.3	25.9	
LF-50-S8	173	157		-2.70E-05	21.0	23.2	
LF-50-S9	223	182		-2.54E-05	31.8	18.4	
LF-50-S10	225	190		-3.03E-05	27.4	31.3	
LF-50-S11	148	127		-8.79E-06	21.4	25.8	
LF-50-S12	237	244		-3.18E-05	30.4	29.8	
LF-50-S13	213	192		-3.15E-05	28.6	24.7	
LF-50-S14	184	203		-7.38E-06	27.0	37.9	
LF-30-S1	165	162		-1.22E-06	25.3	17.6	
LF-30-S2	272	275		-3.18E-06	37.6	37.7	
LF-30-S3	279	250		-5.25E-06	37.1	33.3	
Mean	189	161	81.2	-3.07E-02	25.5	21.9	10.9
Stand. Dev.	52.3	49.9	21.1	9.35E-02	6.54	6.55	2.76
CoV	0.278	0.310	0.259	-3.048	0.256	0.300	0.253

*outlier omitted from analyses

The variation in m_k derived from the results in Table 6 with cyclic range $R = \sigma_r/f_{fi}$ is show Fig. 16(a). It can be seen that there is a negligible reduction in stiffness up to the 70% cyclic range.

The stresses in the cyclic stiffnesses $k_{st\text{-}cy}$, k_{stb} and $k_{1\%}$ in Table 6 have been non-dimensionalised by dividing by the specimens f_{fi} to give $k^*_{st\text{-}cy}$, k^*_{stb} and $k^*_{1\%}$. It can be seen that using the non-dimensional stress σ_r/f_{fi} does give a slight but not significant improvement in the coefficient of variation. The stiffness $k^*_{st\text{-}cy}$ for Specimen LF-50-S5 does appear to be an outlier.

The ascending branch cyclic stiffness $k^*_{st\text{-}cy}$ in Table 6 has a mean value of 25.5 mm^{-1}. Hence when the cyclic range is at its maximum, that is the cyclic peak is at f_{fi}, and the trough at zero, then the change in crack width over this cycle is the inverse of $k^*_{st\text{-}cy}$ which is 0.039 mm. This is an order of magnitude smaller than w_{ffi} from Eq. 5 and two orders of magnitude smaller than that associated with the increase in crack width over the monotonic descending branch in Eq. 1. Hence for all intents and purposes the ascending branch may be considered infinitely stiff that is vertical unless very accurate analyses are required.

From Fig. 16(b), it can be seen that the cyclic stiffness at the start of cyclic loading $k^*_{st\text{-}cy}$ depends on the range of the cyclic load. A linear regression gives

$$k^*_{st-cy} = -17.1R + 34.5 \quad (35)$$

where the units are in mm and in which the standard deviation is

$$SD_{k^*_{st-cy}} = 4.46 \qquad (36)$$

The dependence of the cyclic stiffness at the end of the stable region E_{stb} that is k^*_{stb} is shown in Fig. 16(c) and is given by

$$k_{stb}^{*} = -26.6R + 37.2 \qquad (37)$$

where the units are in mm and the standard deviation is

$$SD_{k_{stb}^{*}} = 5.53 \qquad (38)$$

Finally, the dependence of the cyclic stiffness at $E_{1\%}$ is shown in Fig. 16(d) where the stiffness now increases with range such that

$$E_{1\%}^{*} = 12.5R + 2.49 \qquad (39)$$

and where the units are in mm and the standard deviation is

$$SD_{k_{1\%}^{*}} = 2.41 \qquad (40)$$

Crack development

Crack width bounds and fracture energy

The mean of the monotonic crack width for the descending branch from Eq. 1 is plotted in Fig. 17 as the line B-C and labelled $w_{mon\text{-}mn}$. The ascending branch A-B labelled $w_{ffi\text{-}mn}$ from Eq. 5 has been shown for all intents and purposes to be vertical. Hence A-B-C is both an envelope of the mean crack widths and importantly the enclosed area is the fracture energy. Also plotted is the bound from Eq. 24 that governs the transition from stable to unstable crack propagation; when x is zero in Eq. 24, this gives the mean value A-J-K which is labelled $w_{stb\text{-}mn}$. In plotting these bounds the upper limit of the monotonic envelope has not been considered and hence they are shown to extend beyond A-B-C.

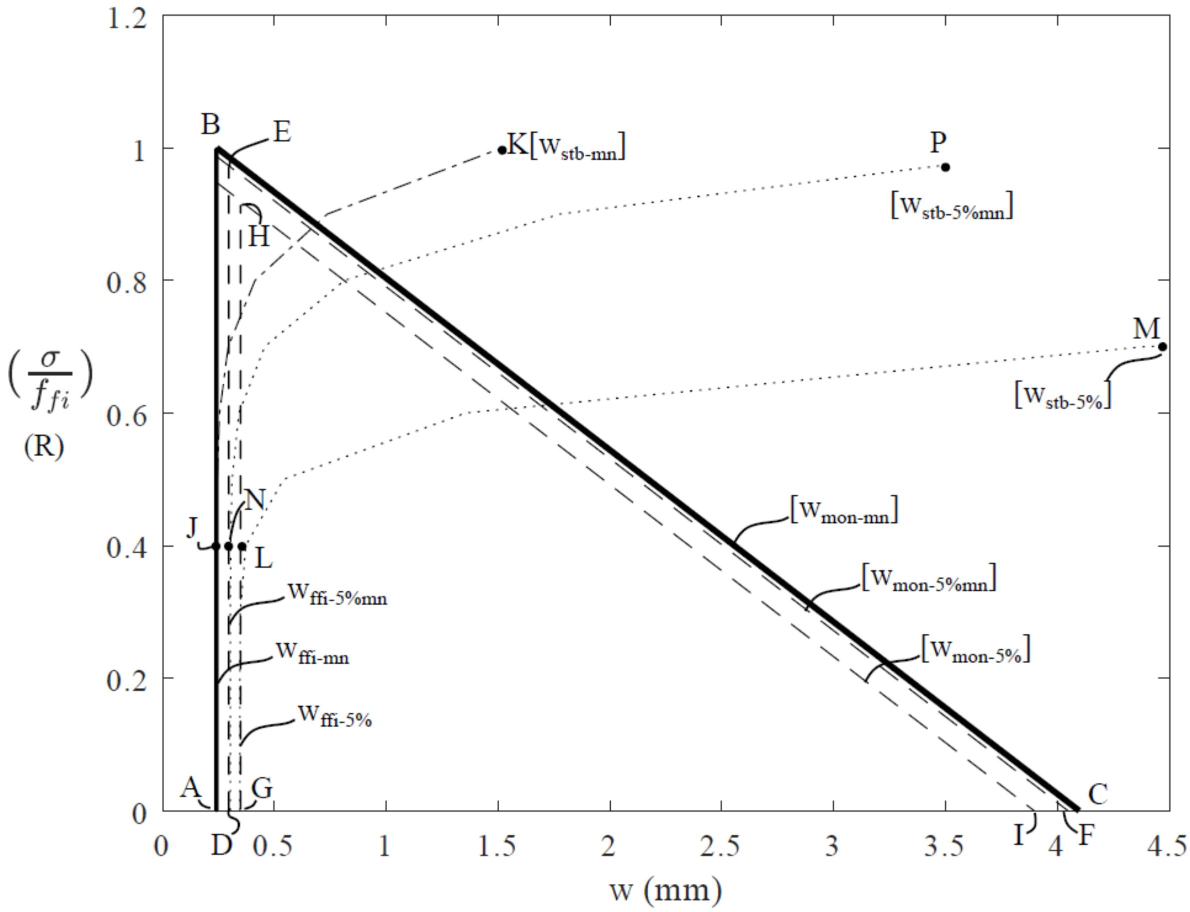

Fig. 17 Crack width bounds

Characteristic values are generally used in design. From the standard deviations of Eqs. 1 and 5 given in Eqs. 2 and 6, the 5% confidence limits, that is at x = 1.64 in the equations, gives the envelope G-H-I and the bound G-L-M. These bounds are for a cracked cross-section of UHPFRC of 80 mm x 80 mm as used in the tests. This is a very small area compared with a cracked surface in a beam or slab and could, therefore, be considered to give an over conservative design. As can be seen from the monotonic descending branch B-C, UHPFRC behaves in reasonable ductile fashion. Because of this ductility, it is suggested that the statistical theory of the standard error of the mean can be applied. Hence and as an example, if it is assumed that the surface area of the crack in the beam or slab is 16 times that of the tension specimen tested, then the standard error is SD/√16 that is ¼ SD. Using this standard deviation gives the bounds D-E-F and D-N-P. It is felt that this approach would be more suitable and less over-conservative for design but it is only a suggestion.

Crack propagation

The bounds for the SD/4 in Fig. 17 are shown in Fig. 18 although the following approach could be applied to any bounds. On cracking, the initial crack width is w_{ffi} at Point A as shown.

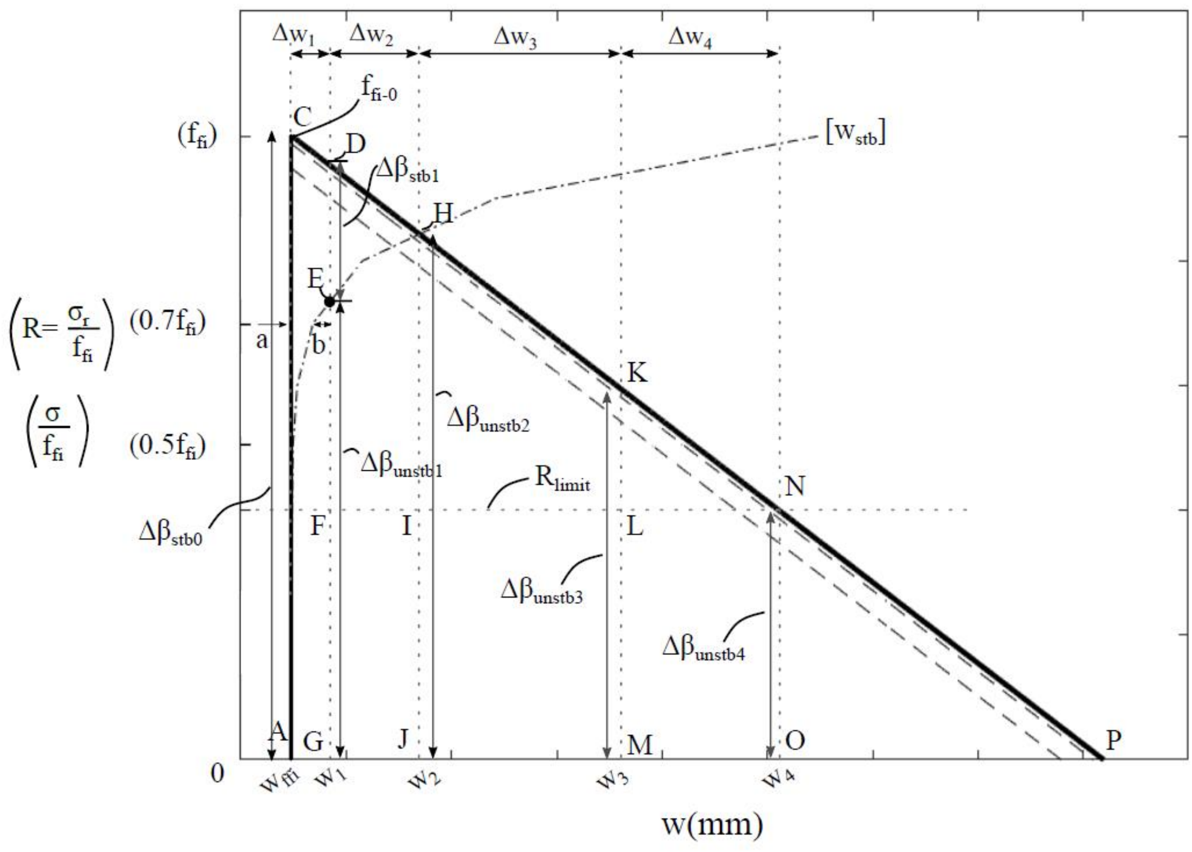

Fig. 18 Crack accumulation

Let us consider how the crack can be widened by Δw_1 in Fig. 18 There are two ways the crack width can be increased. A tensile displacement could be applied. In this case, the stress would increase from zero to f_{fi} that is from A to C. Then under further displacement control, the crack would widen by say Δw_1 as shown and the stress would reduce to that at Point D which is the residual strength and where the crack width is w_1.

Alternatively a cyclic load could be applied and, through the incremental set, the crack could widen until Δw_1 is achieved. On first applying the cyclic load, β_{stb} governs all the ranges and this is shown as $\Delta\beta_{stb0}$. However, it can be seen that when Δw_1 is achieved, the range between D and E is controlled by β_{stb} and this has been labelled $\Delta\beta_{stb1}$ and the remaining range between E and G is controlled by β_{unstb} and labelled $\Delta\beta un_{stb1}$. Hence if a range between G and E were applied such as that at R = 0.7, then the initial incremental set would be controlled by β_{stb} for R = 0.7 until the increase in crack width '*a'* that can be derived from Eq. 13 reached the bound from Eq. 24, after which the crack development '*b'* would be governed by β_{unstb} and given by Eq. 19. It is suggested that a way of visualising the behaviour is that, whether the increase in crack width is due to an applied displacement or cyclic loads or both, the specimen ends up with the same properties defined by D-E-G.

The above mechanisms can be applied to further widen the crack Δ_{w2} in Fig. 18 where the residual strength has reduced to that at Point H, after which it can be seen that crack propagation is controlled solely by β_{unstb}. It can be seen that whether a crack is widened through displacement control or cyclic loading, the progression along the monotonic descending branch can be quantified.

Concept of fatigue limit

A fatigue limit could be defined as a bound for safe cyclic loads, that is cyclic loads that do not cause fatigue damage. From the stable incremental set β_{stb} values in Table 5, it can be seen that at the $0.3f_{fi}$ range, that is for Specimens LF-30-S1 to LF-30-S3, $\beta_{stb\text{-}mn}$ is miniscule at a mean value of 1.061E-10 suggesting that there is virtually no fatigue damage. For the series with a range of $0.5f_{fi}$, there are two results LF-50-S1 and LF-50-S2 where there was no fatigue damage but the remainder did have fatigue damage although very small. Hence a fatigue limit could conceptually lie at a smaller range. It is suggested that a fatigue limit could be placed at a range of approximately $0.4f_{fi}$, the log of which is -0.4 as shown in Fig. 13(a). The associated crack width at this fatigue limit being given by Eq. 24.

The above fatigue limit is based on the stable incremental set when damage is purely due to cyclic loading, that is the permanent increase in crack width is due to cyclic loading. As has been explained above, permanent damage can also be caused by monotonic loading that follows the descending monotonic branch. In which case, should the increase in the crack width due to monotonic loading exceed that given by Eq. 24 which is based on the stable incremental set, then the fatigue limit is exceeded and crack widening is defined by the unstable incremental set. It can be seen that the fatigue limit can be exceeded prior to cyclic loading due to monotonic loading. Hence the concept of a fatigue limit cannot be applied safely when dealing with cracked fibre concrete.

Conclusions

A technique for quantifying the material properties across a crack in UHPFRC when subjected to both monotonic and cyclic loads has been developed. As an example, this technique has been applied to a UHPFRC with 13mm high strength steel fibres which had a compressive strength of 166MPa and in which debonding is the only failure mode. The technique is based on the maximum strength after cracking as using this property to control the applied monotonic and cyclic loads was found to reduce the scatter of results.

It was found that the monotonic descending branch of the stress/crack-width relationship provided a very good envelope for the cyclic behaviour. The cyclic behaviour was governed by the range of the cyclic stress which controlled the increase in crack width per cycle that is the incremental set. Furthermore, the incremental set consisted of a stable region in which the crack width increased uniformly and an unstable region in which the crack width increased rapidly. It was shown that the stable and unstable incremental sets and the number of cycles or bounds in which they occurred could be quantified. It was also shown how the incremental set cyclic properties could be used with the monotonic properties to quantifying the behaviour across a cracked plane in UHPFRC, that is, it could be used to predict the fatigue behaviour when subjected to any combination of monotonic and cyclic loads.

While the techniques presented for testing and quantifying the fatigue behaviour of UHPFRC are generic, the material model presented is unique to the individual mix design. It is recommended that further experimental testing is required covering a broad range of concrete and fibre properties before a generic material model can be developed.

Data availability statement

All data, models, and code generated or used during the study appear in the submitted article.

Acknowledgements

This material is based upon work supported by the Australian Research Council Discovery Project 190102650"

Notation

$A_{cr\text{-}pl}$	cross-sectional area of cracked plane
CF	cycled to failure
CL	confidence limit
dw/dN	incremental set
F	force
F_B, F_T	internal forces in the concrete, respectively bottom and top.
FL	fatigue limit
f_c	concrete compressive cylinder strength
f_{ctsp}	concrete tensile strength from tension specimen from load to cause cracking
f_{fi}	monotonic tensile fibre strength from tension specimens
$f_{fi\text{-}cy}$	tensile fibre strength after cyclic loading; residual strength after cyclic loading
E_c	concrete modulus from standard test in code
E_{stb}	endurance at the end of the stable incremental set β_{stb}
$E_{stb\text{-}curv}$	E_{unstb} from a linear analysis
$E_{unstb\text{-}curv}$	E_{unstb} from a curvilinear analysis
$E_{unstb\text{-}lin}$	E_{unstb} from a linear analysis
$E_{1\%}$	endurance when σ_{pk} has reduced by 1%
k	cyclic stiffness of ascending branch (N/mm^3)
k_{stb}	k at E_{stb}
$k_{st\text{-}cy}$	k at start of cyclic loading
$k_{1\%}$	k at $E_{1\%}$

k^*	k/f_{fi}
$k^*_{st\text{-}cy}$	$k_{st\text{-}cy}/f_{fi}$
k^*_{stb}	k_{stb}/f_{fi}
$k^*_{1\%}$	$k_{1\%}/f_{fi}$
LF	loaded to failure
M	monotonic; normalised mean cyclic stress σ_m/f_{fi}
m_k	slope of variation in k with N
N	cycle; cycle number
N_{blk}	number of cycles applied in a block
NE	northeast
NW	northwest
P	cyclic peak; σ_{pk}/f_{fi}
R	cyclic range; $(\sigma_{pk}-\sigma_{tr})/f_{fi}$
R_{tran}	range at transition of bilinear variation
S	specimen
SD	standard deviation
$SD_{des\text{-}lin}$	SD of descending branch from linear analysis
$SD_{des\text{-}non}$	SD of descending branch from non-linear analysis
SD_{wffi}	SD of the monotonic crack width at f_{fi}
$SD_{\beta stb\text{-}lin}$	SD for stable incremental set linear analysis
$SD_{\beta unstb\text{-}lin}$	SD for unstable incremental set linear analysis
$SD_{Estb\text{-}lin}$	SD for stable endurance linear analysis
$SD_{Eunstb\text{-}lin}$	SD for unstable endurance linear analysis
$SD_{\beta stb\text{-}curv}$	SD for stable incremental set curvilinear analysis
$SD_{\beta unstb\text{-}curv}$	SD for unstable incremental set curvilinear analysis

$SD_{Estb\text{-}curv}$	SD for stable endurance curvilinear analysis
$SD_{Eunstb\text{-}curv}$	SD for unstable endurance curvilinear analysis
$SD_{k^*_{st-cy}}$	SD for cyclic stiffness analysis at the start of cyclic loading
$SD_{k^*_{stb}}$	SD for cyclic stiffness analysis at the end of the stable region
$SD_{k^*_{1\%}}$	SD for cyclic stiffness analysis at $E_{1\%}$
SE	southeast
SW	southwest
T	cyclic trough; σ_{tr}/f_{fi}
UHPC	ultra high performance concrete
UHPFRC	ultra high performance fibre reinforced concrete
w	width of crack; average crack width
w_{crn}	width of crack at corner of cracked face of tension specimen
w_{ffi}	monotonic width of crack at f_{fi}
$w_{ffi\text{-}cy}$	crack width at $f_{fi\text{-}cy}$
$w_{mon\text{-}mn}$	mean of the monotonic crack width descending branch
$w_{ffi\text{-}mn}$	mean crack width at mean f_{fi}
w_{Nblk}	crack width after a block of N_{blk} cycles and prior to loading to failure
w_{stb}	crack width at the end of stable incremental set
$w_{stb\text{-}mn}$	mean crack width at the end of stable incremental set
$w_{1\%}$	crack width when σ_{pk} has reduced by 1%; crack width at $E_{1\%}$
x	number of SD required for CL
β	incremental set; dw/dN
β_{stb}	stable incremental set
$\beta_{stb\text{-}curv}$	β_{stb} from curvilinear analysis
$\beta_{stb\text{-}lin}$	β_{stb} from linear analysis

β_{stb-mn} mean of β_{stb}

$\beta_{stb-mn-curv}$ β_{stb-mn} from curvilinear analysis

$\beta_{stb-mn-lin}$ β_{stb-mn} from linear analysis

β_{unstb} unstable incremental set

$\beta_{unstb-curv}$ β_{unstb} from curvilinear analysis

$\beta_{unstb-lin}$ β_{unstb} from linear analysis

σ stress

σ_m cyclic stress at mean of cycle

σ_{pk} cyclic stress at peak of cycle

σ_R range of cyclic stresses

σ_r cyclic range of stress

σ_{tr} cyclic stress at trough of cycle

Δw_{stb} increase in crack width due to β_{stb}

$\Delta w_{stb-lin}$ Δw_{stb} from linear analysis

Δw_{tran} increase in crack width at transition from stable to unstable region

$\Delta w_{unstb-lin}$ increase in crack width due to $\beta_{unstb-lin}$

$\Delta\beta_{stb}$ region over which β_{stb} applies

$\Delta\beta_{unstb}$ region over which β_{unstb} applies

Supplementary Material

Figures S1-S21 are available online in the ASCE library.

References

Abbas, S., Nehdi, M. L., and Saleem, M. A. (2016). “Ultra-High Performance Concrete:

Mechanical Performance, Durability, Sustainability and Implementation Challenges." *International Journal of Concrete Structures and Materials*, 10(3), 271–295.

Azmee, N. M., and Shafiq, N. (2018). "Ultra-high performance concrete: From fundamental to applications." *Case Studies in Construction Materials*, Elsevier, 9, 1–15.

Carlesso, D. M., de la Fuente, A., and Cavalaro, S. H. P. (2019). "Fatigue of cracked high performance fiber reinforced concrete subjected to bending." *Construction and Building Materials*, Elsevier, 220, 444–455.

Comité Euro-International du Béton (CEB). (1996). *RC elements under cyclic loading -State-of-the-art report*. London.

Cornelissen, H. A. W. (1984). *Fatigue failure of concrete in tension*. Heron, Delft, The Netherlands.

Germano, F., Tiberti, G., and Plizzari, G. (2016). "Post-peak fatigue performance of steel fiber reinforced concrete under flexure." *Materials and Structures/Materiaux et Constructions*, Springer Netherlands, 49(10), 4229–4245.

González, D. C., Moradillo, R., Mínguez, J., Martínez, J. A., and Vicente, M. A. (2018). "Postcracking residual strengths of fiber-reinforced high-performance concrete after cyclic loading." *Structural Concrete*, 19(2), 340–351.

Isojeh, B., El-Zeghayar, M., and Vecchio, F. J. (2017). "Fatigue behavior of steel fiber concrete in direct tension." *Journal of Materials in Civil Engineering*, 29(9), 04017130-1–9.

Lee, M. K., and Barr, B. I. G. (2004). "An overview of the fatigue behaviour of plain and fibre reinforced concrete." *Cement and Concrete Composites*, Elsevier, 26(4), 299–305.

Makita, T., and Brühwiler, E. (2014). "Tensile fatigue behaviour of ultra-high performance fibre reinforced concrete (UHPFRC)." *Materials and Structures*, 47(3), 475–491.

Naaman, A. E., and Hammoud, H. (1998). "Fatigue characteristics of high performance fiber-reinforced concrete." *Cement and Concrete Composites*, 20(5), 353–363.

Oehlers, D. J., and Bradford, M. A. (1995). *Composite steel and concrete structural members: Fundamental behaviour*. Pergamon.

Russell, H. G., and Graybeal, B. A. (2013). *Ultra-high Performance Concrete: A State-of-the-Art Report for the Bridge Community.* Springfield, VA.

Singh, M., A. H. Sheikh, M. S. Mohamed Ali, P. Visintin, and M. C. Griffith. (2017). "Experimental and Numerical Study of the Flexural Behaviour of Ultra-high Performance Fibre Reinforced Concrete Beams." *Construction and Building Materials* 138: 12–25.

Sohail, M. G., Wang, B., Jain, A., Kahraman, R., Ozerkan, N. G., Gencturk, B., Dawood, M., and Belarbi, A. (2018). "Advancements in concrete mix designs: High-performance and ultrahigh-performance concretes from 1970 to 2016." *Journal of Materials in Civil Engineering*, 30(3), 04017310-1–20.

Voo, Y. L., Foster, S. J., and Voo, C. C. (2015). "Ultrahigh-Performance Concrete Segmental Bridge Technology: Toward Sustainable Bridge Construction." *Journal of Bridge Engineering*, 20(8), B5014001-1–12.

Yang, I. H., Joh, C., and Kim, B. S. (2010). "Structural behavior of ultra high performance concrete beams subjected to bending." *Engineering Structures*, Elsevier Ltd, 32(11), 3478–3487.

Zhang, J., Stang, H., and Li, V. C. (2000). "Experimental study on crack bridging in frc under uniaxial fatigue tension." *Journal of Materials in Civil Engineering*, 12(1), 66–73.

Supplementary material

Direct tension tests were performed on un-notched dogbane specimens (Figure S1) to quantify the tensile properties of the concrete when not influenced by the notch. The specimens, which have previously been tested by Singh et al. (2017) and Visintin et al. (2018), have an overall length of 605 mm, a test region of length 300 mm and a cross-section of 100 mm x 100 mm. Specimens were loaded under displacement control at a 0.05 mm/min until a displacement of 1.5 mm, after this the rate was increased to 0.2 mm/min till 4 mm, and then 1 mm/min was used. Throughout testing, the total elongation of the 300 mm test region region was measured using 4 LVDTs as shown in Fig. S1.

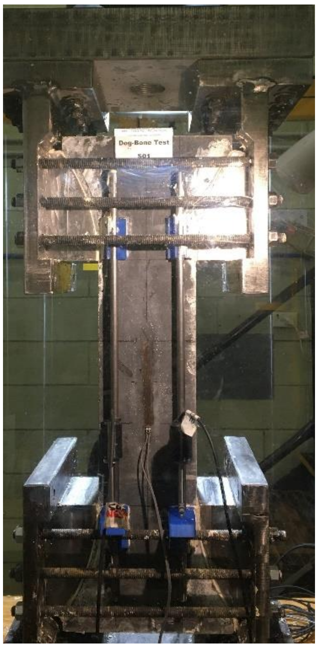

Fig S1: un-notched direct tension test specimen

Six specimens were tested when the concrete was between 140 and 151 days old, and the results are summarised in Fig. S2.

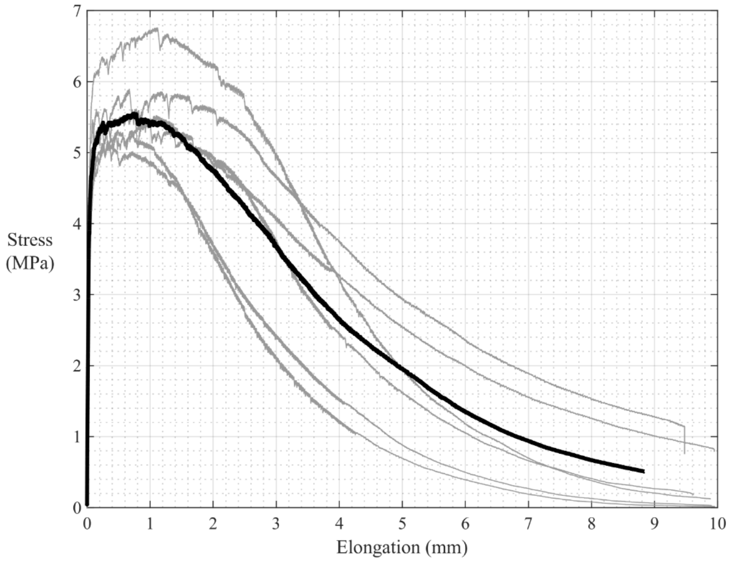

Fig S2: un-notched direct tension test results

The cyclic-stress/crack-widths, as already explained in the main body in Fig. 7, for all the specimens tested are presented in Figs. S3-S9 and have been compared with the monotonic descending branch from Eqs. 1 and 3.

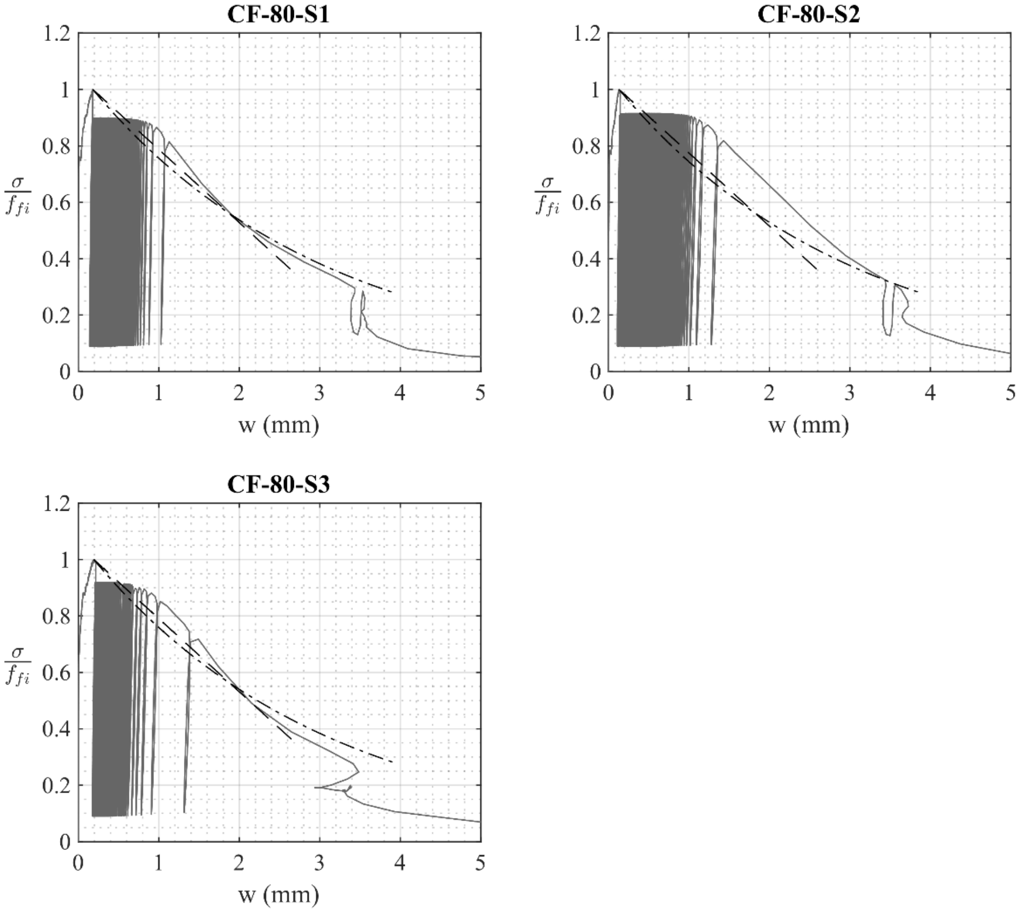

Fig. S3: Cycled to failure test data at (a) 80% range

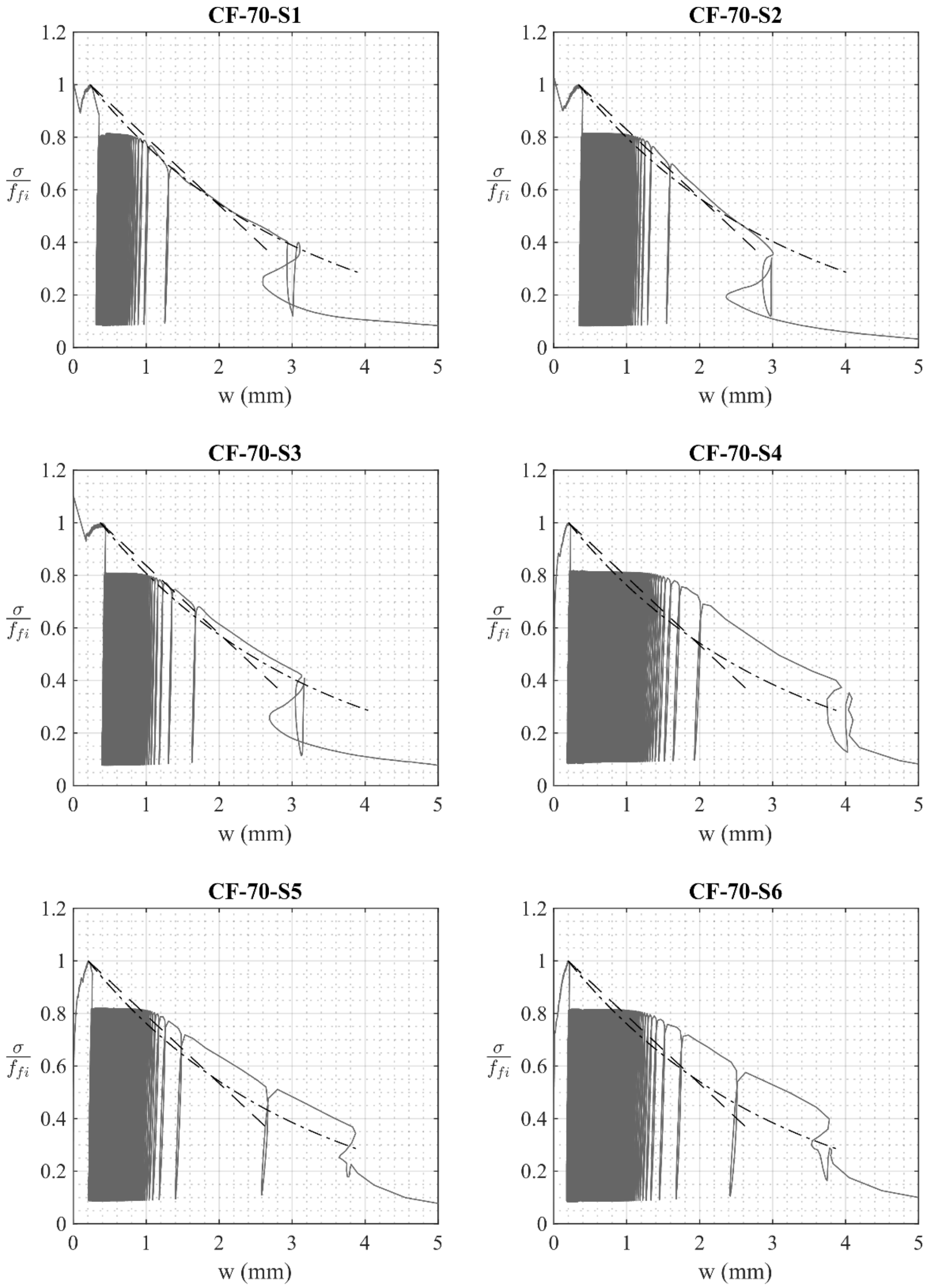

Fig. S4: Cycled to failure test data at (a) 70% range

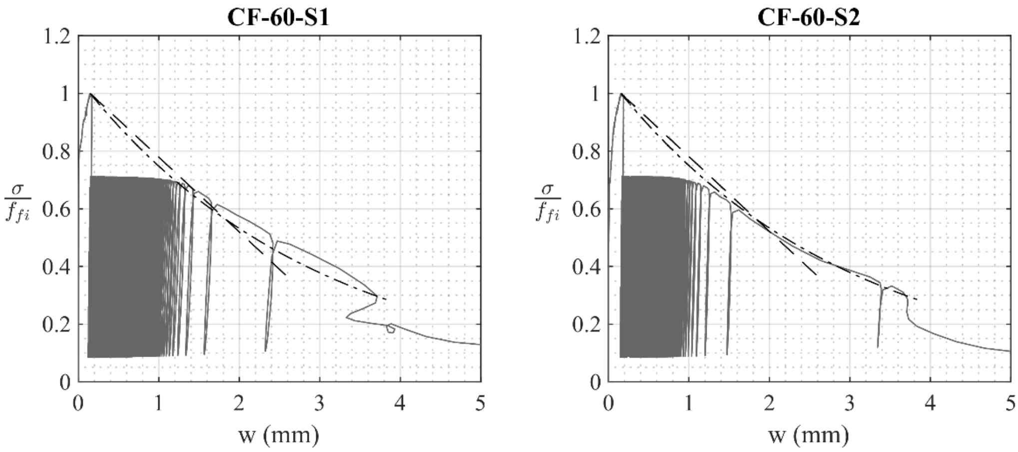

Fig S5: Cycled to failure test data at 60% range

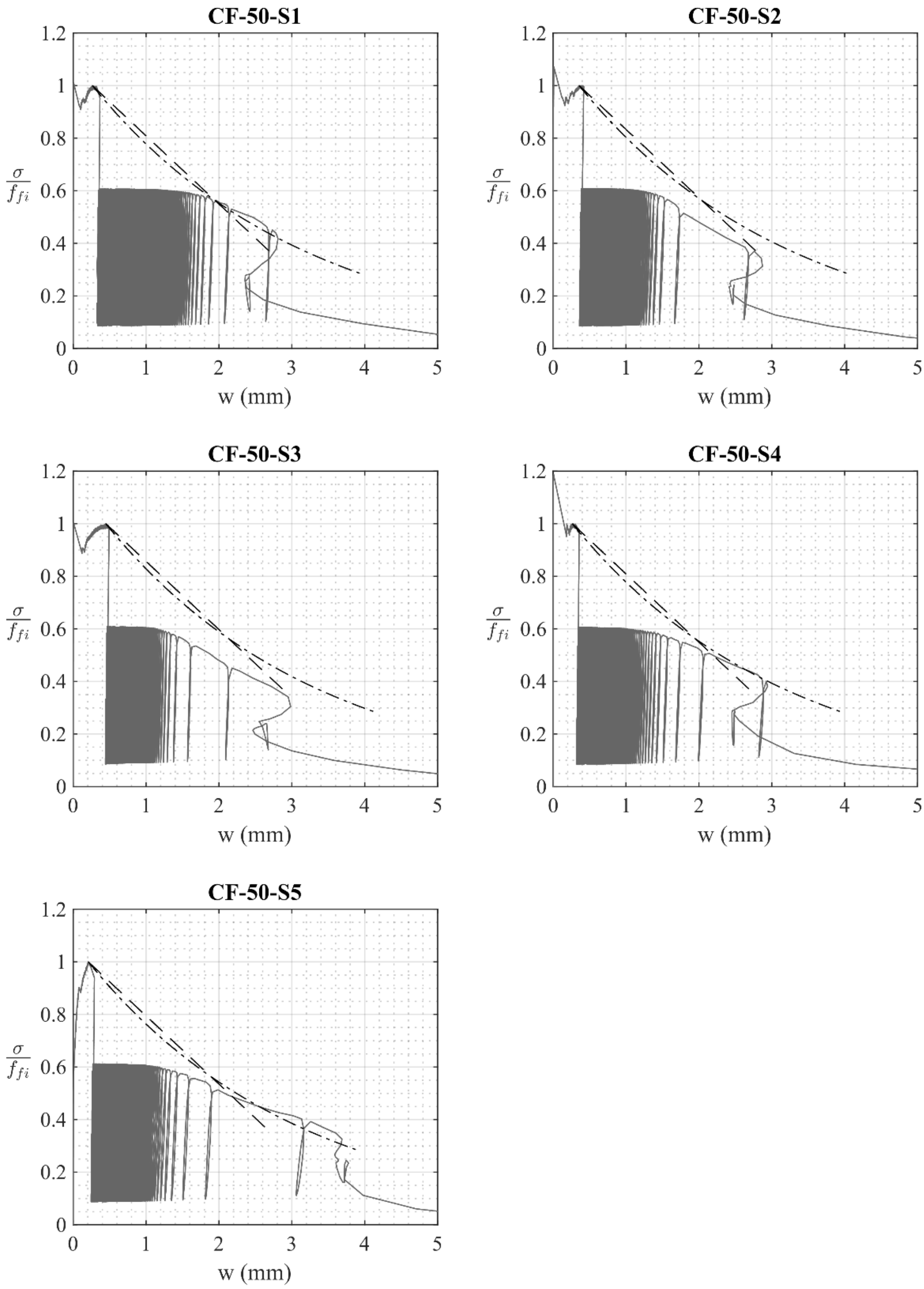

Fig S6: Cycled to failure test data at 50% range

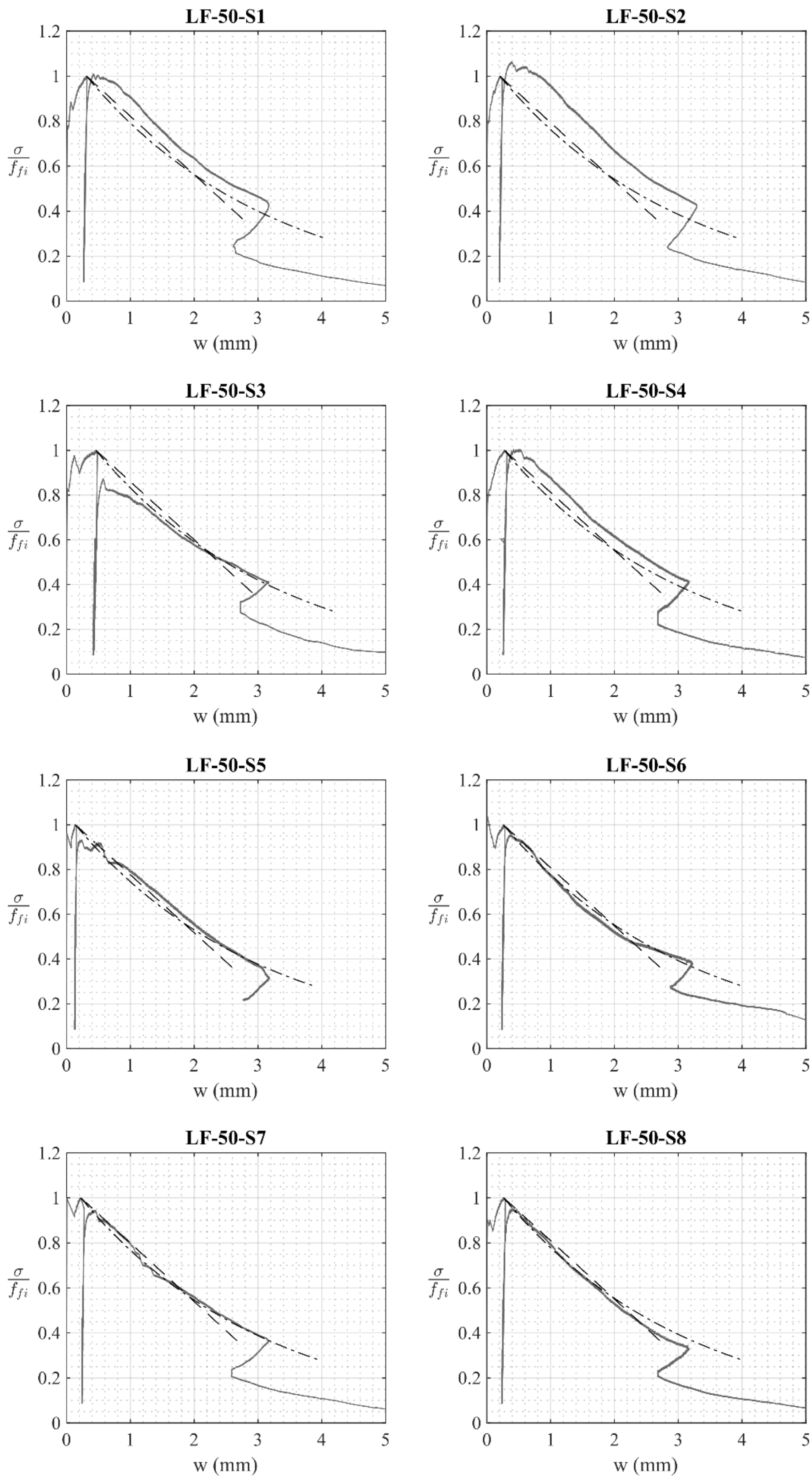

Fig S7: Loaded to failure test data at 50% range (samples 1-8)

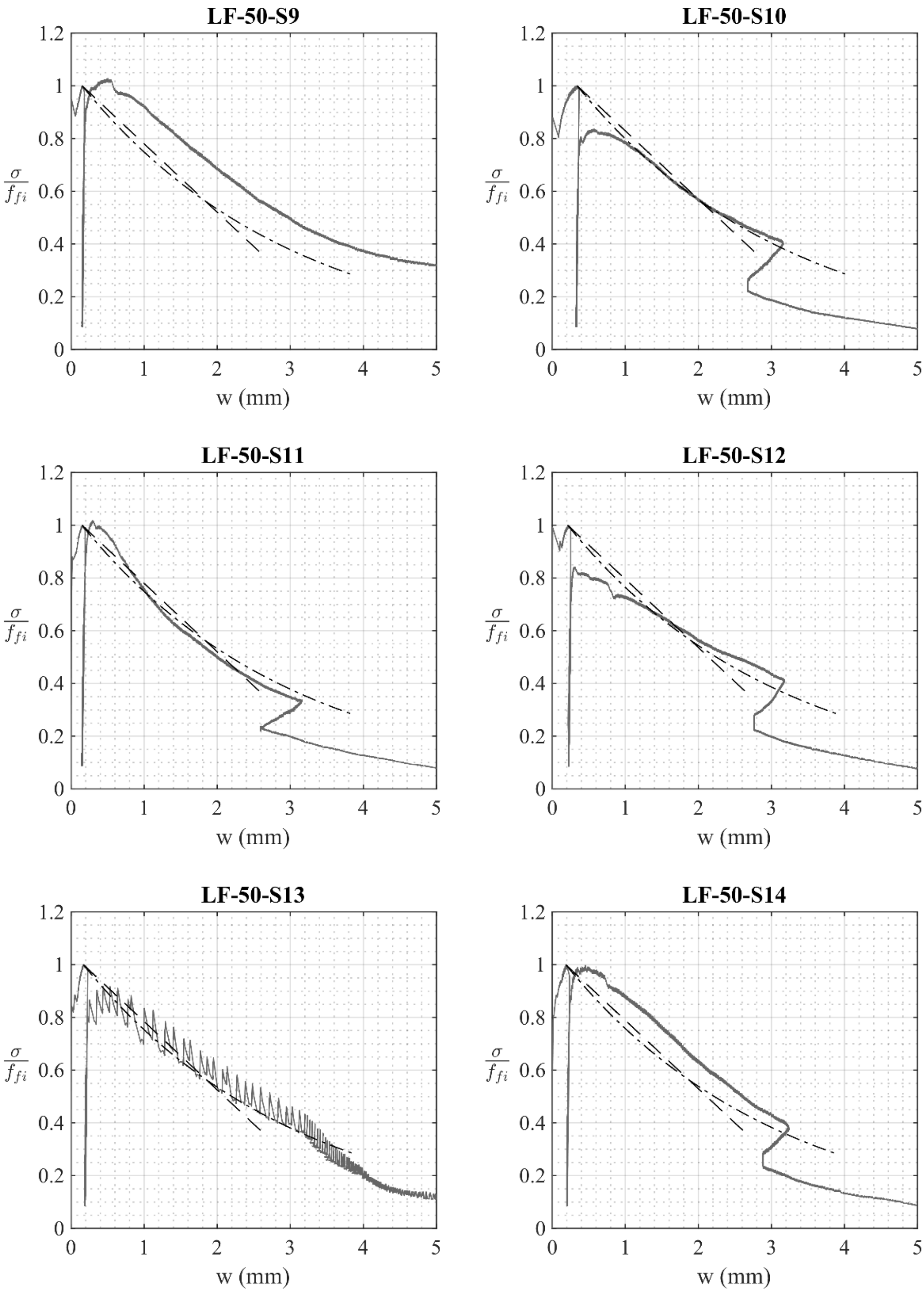

Fig S8: Loaded to failure test data at 50% range (samples 9-14)

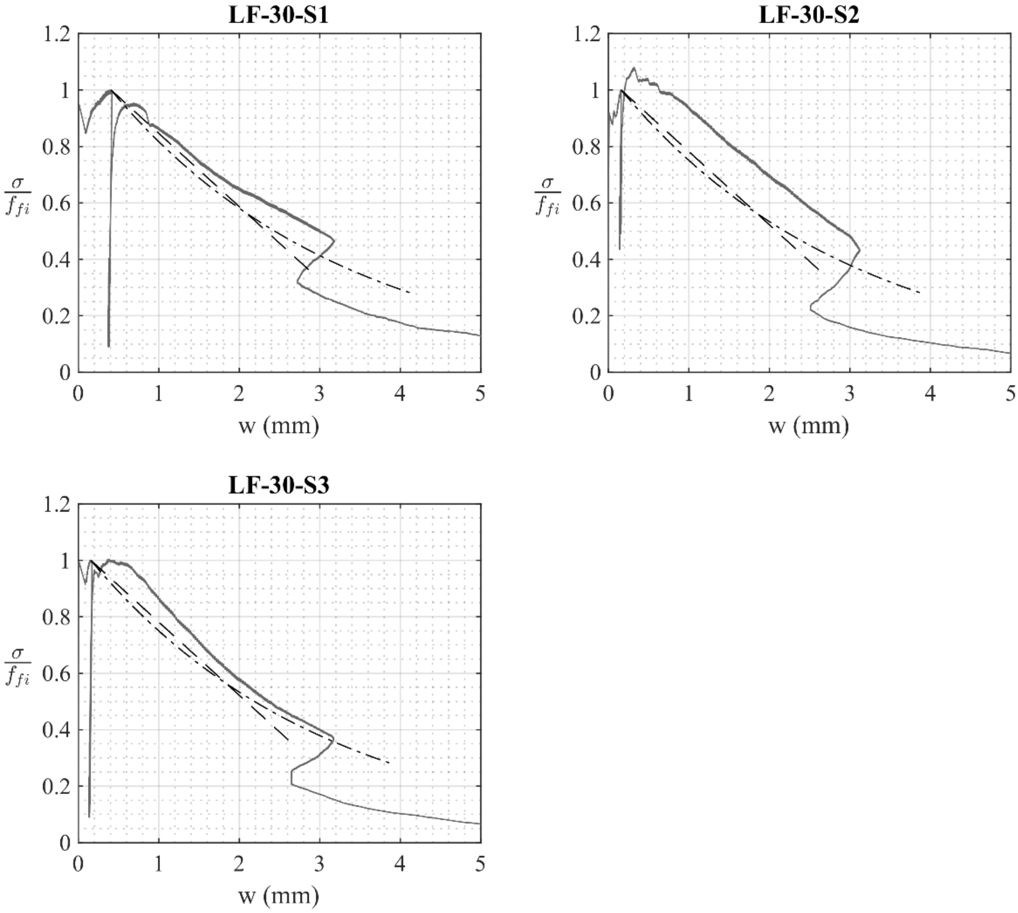

Fig S9: Loaded to failure test data at 30% range

The analysis of all the fatigue data to extract the incremental set, as explained in Figs. 11 and 12, are presented in Figs. S10-S16. The bold line was used to determine the stable properties.

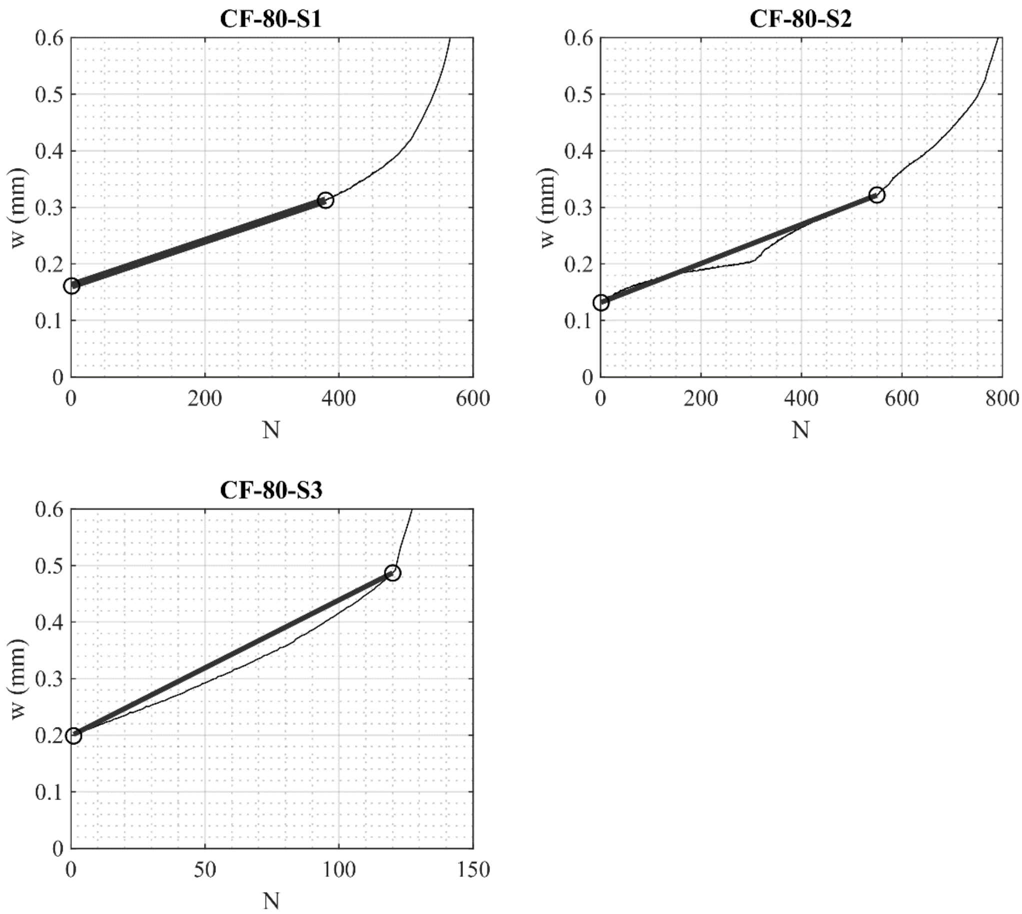

Fig. S10: Variation in crack width, cycled to failure, 80% range

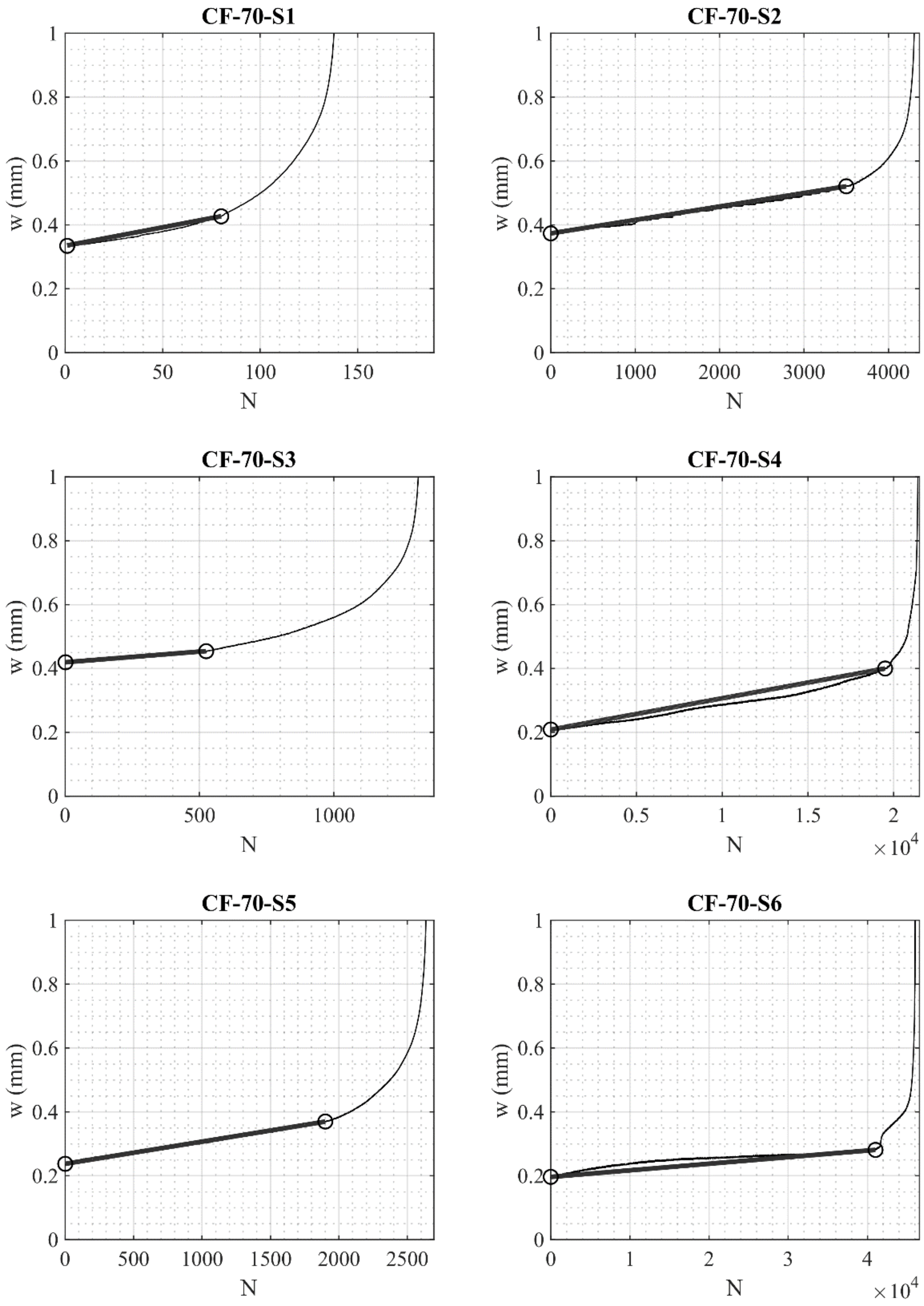

Fig. S11: Variation in crack width, cycled to failure, 70% range

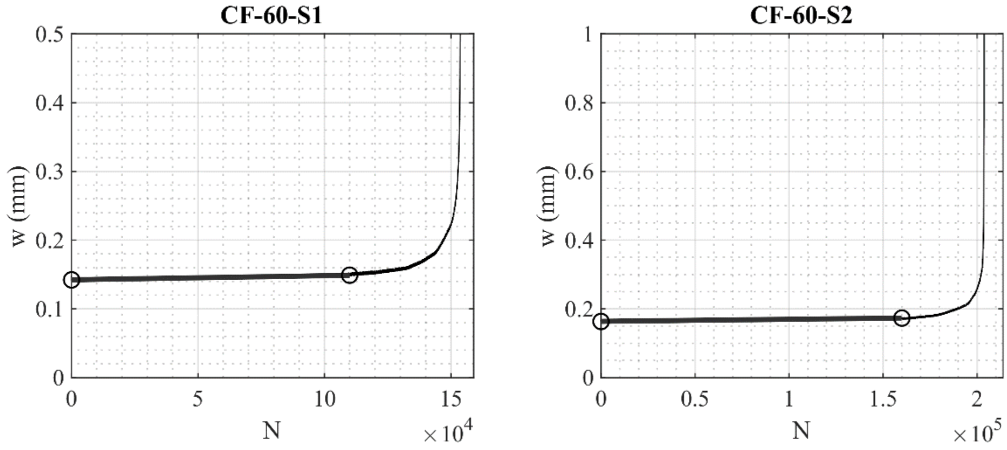

Fig. S12: Variation in crack width, cycled to failure, 60% range

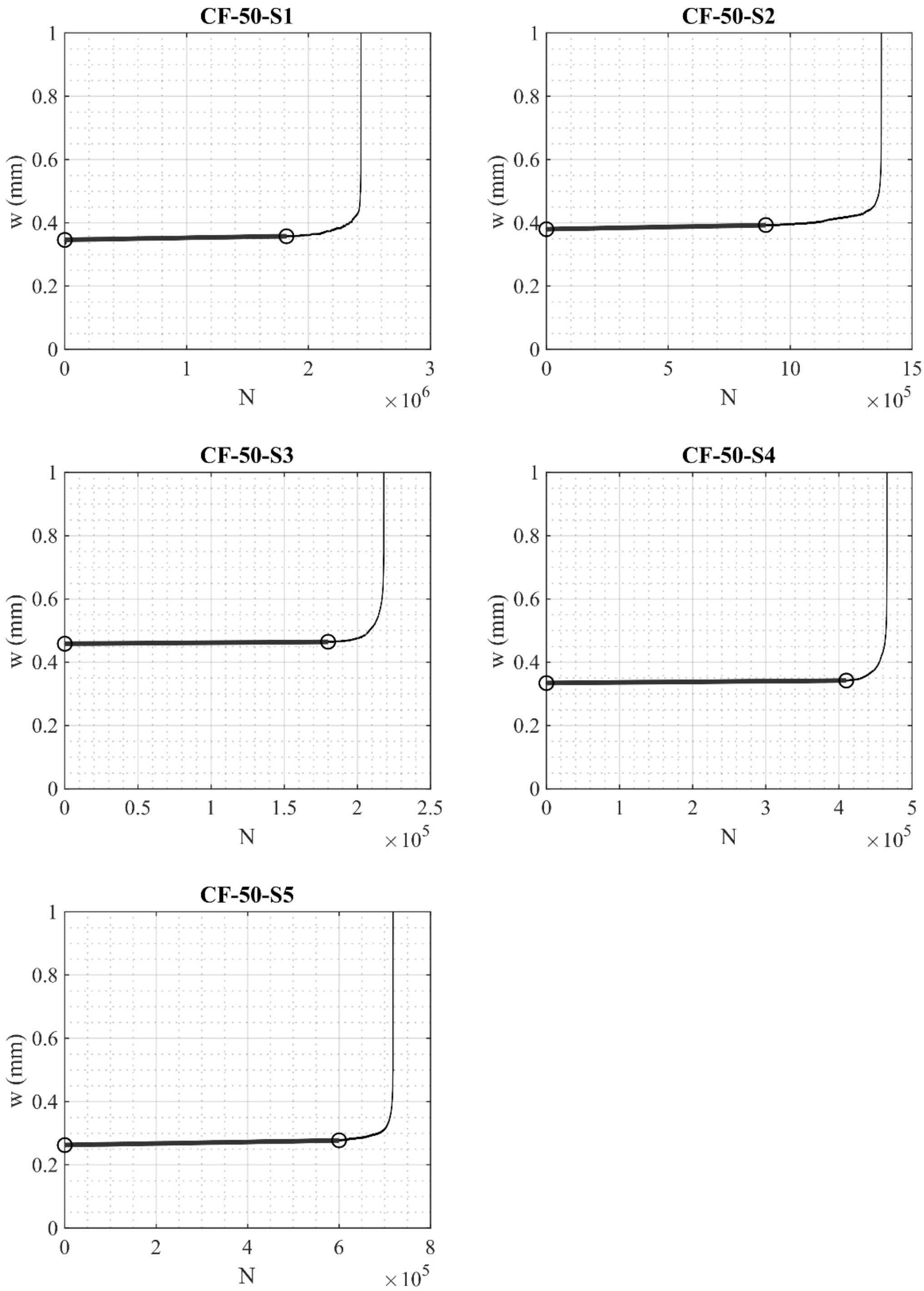

Fig. S13: Variation in crack width, cycled to failure, 50% range

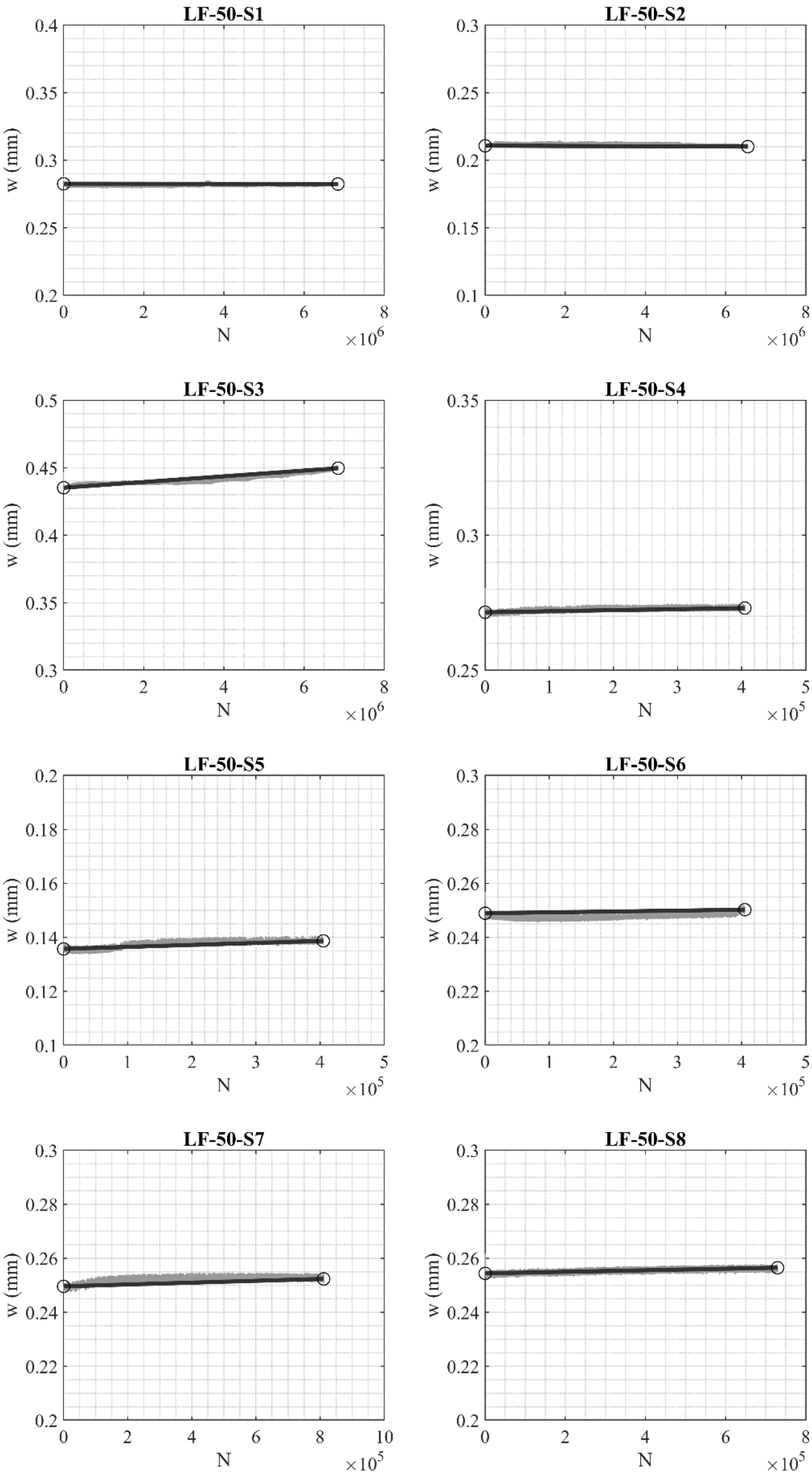

Fig. S14: Variation in crack width, loaded to failure, 50% range (specimens 1-8)

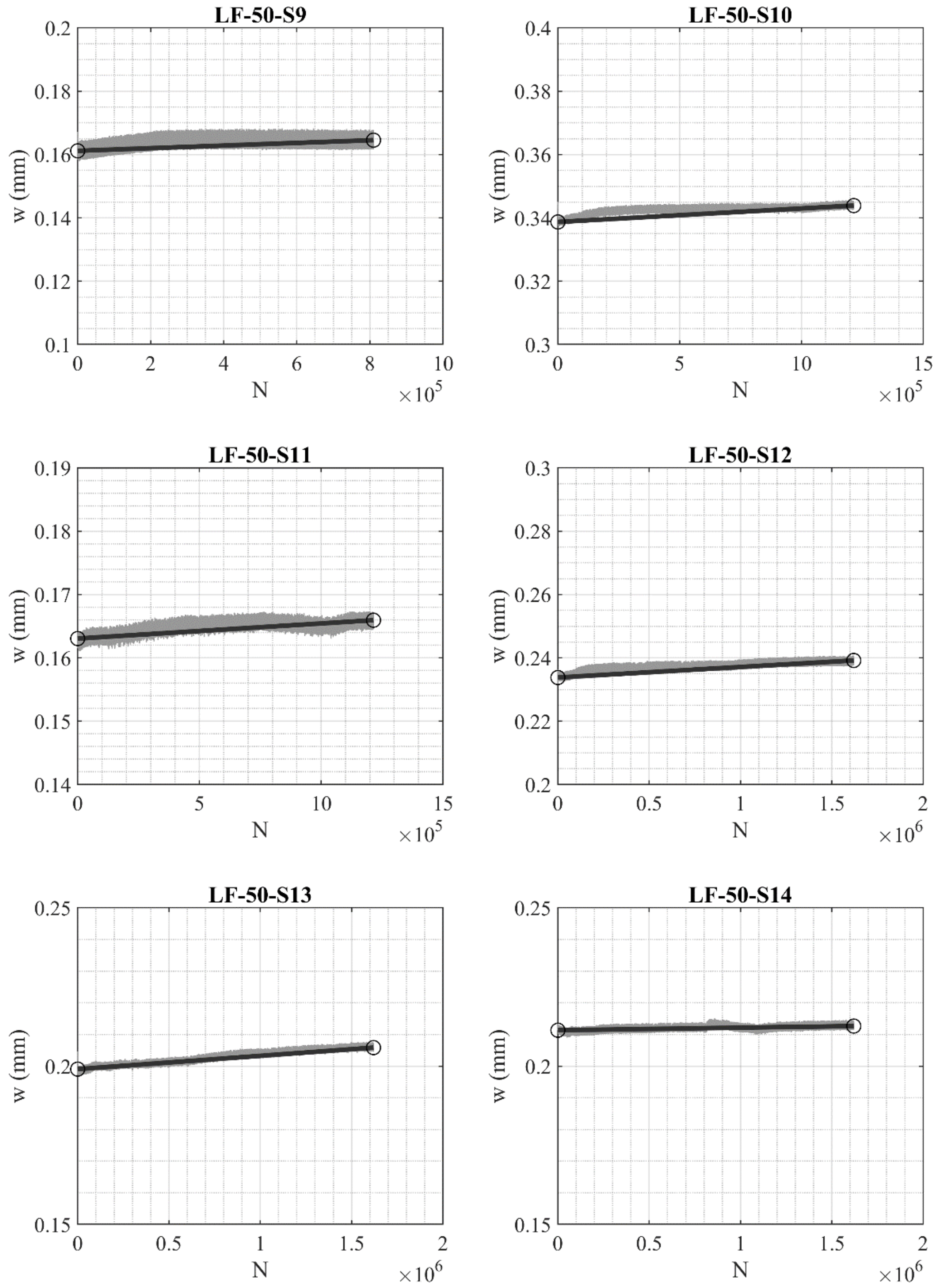

Fig. S15: Variation in crack width, loaded to failure, 50% range (specimens 9-14)

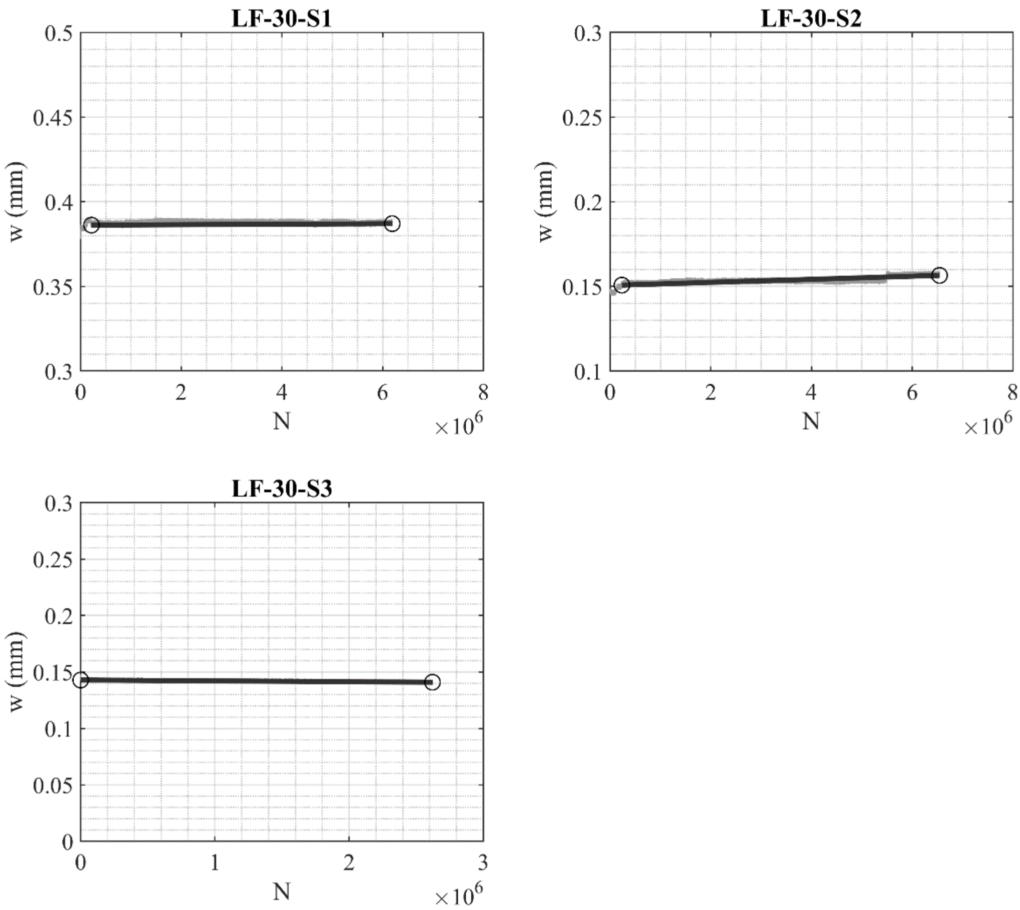

Fig. S16: Variation in crack width, loaded to failure, 30% range

The analysis of all the fatigue data to extract the cyclic stiffness, as explained in Fig. 15 are presented in Figures S17-S23. The bold line was used to determine the stiffness properties.

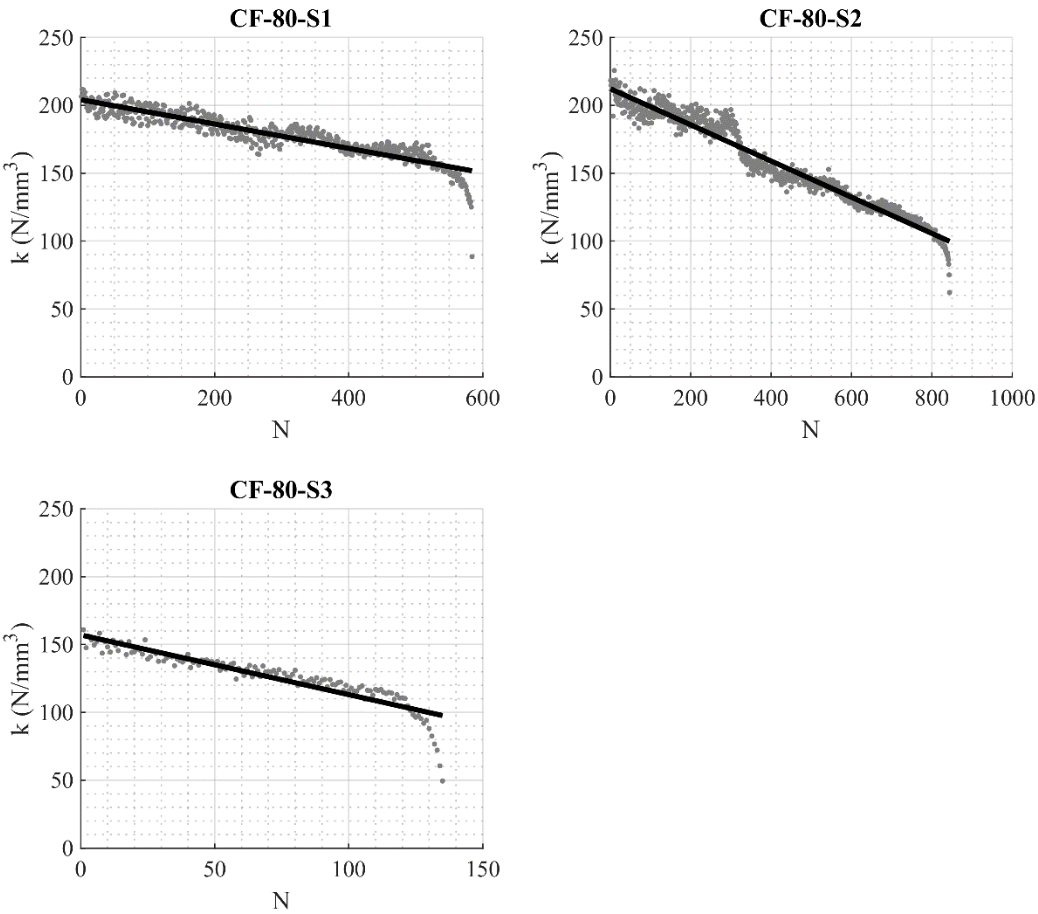

Fig. S17: Variation in cyclic stiffness 80% range

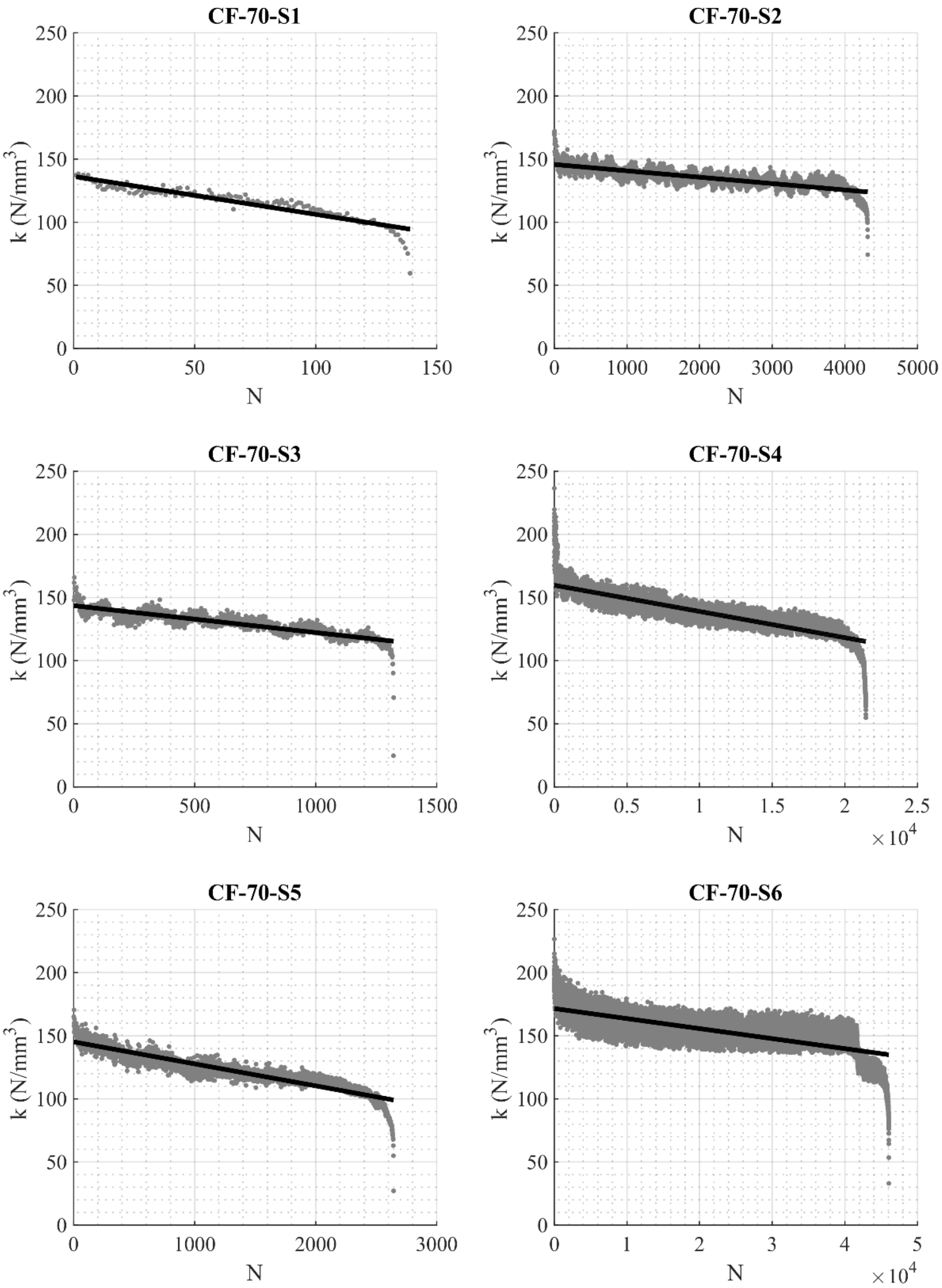

Fig. S18: Variation in cyclic stiffness 70% range

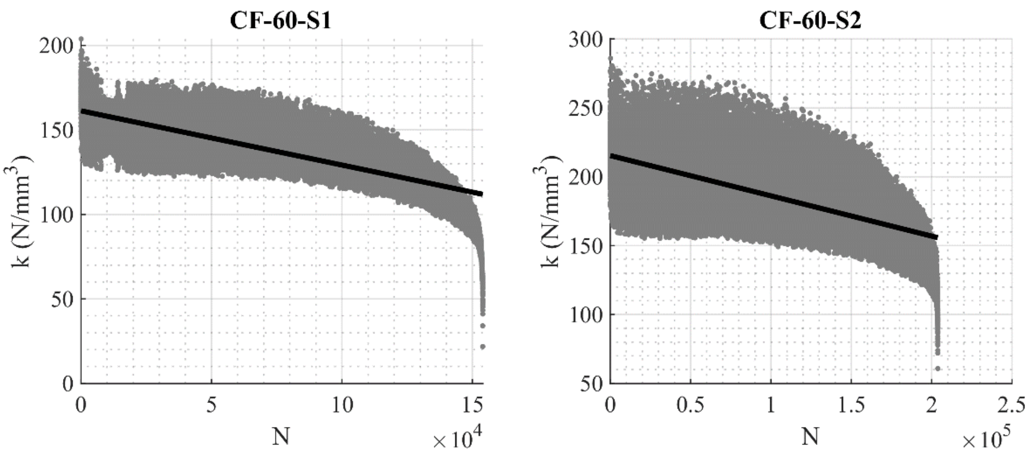

Fig. S19: Variation in cyclic stiffness 60% range

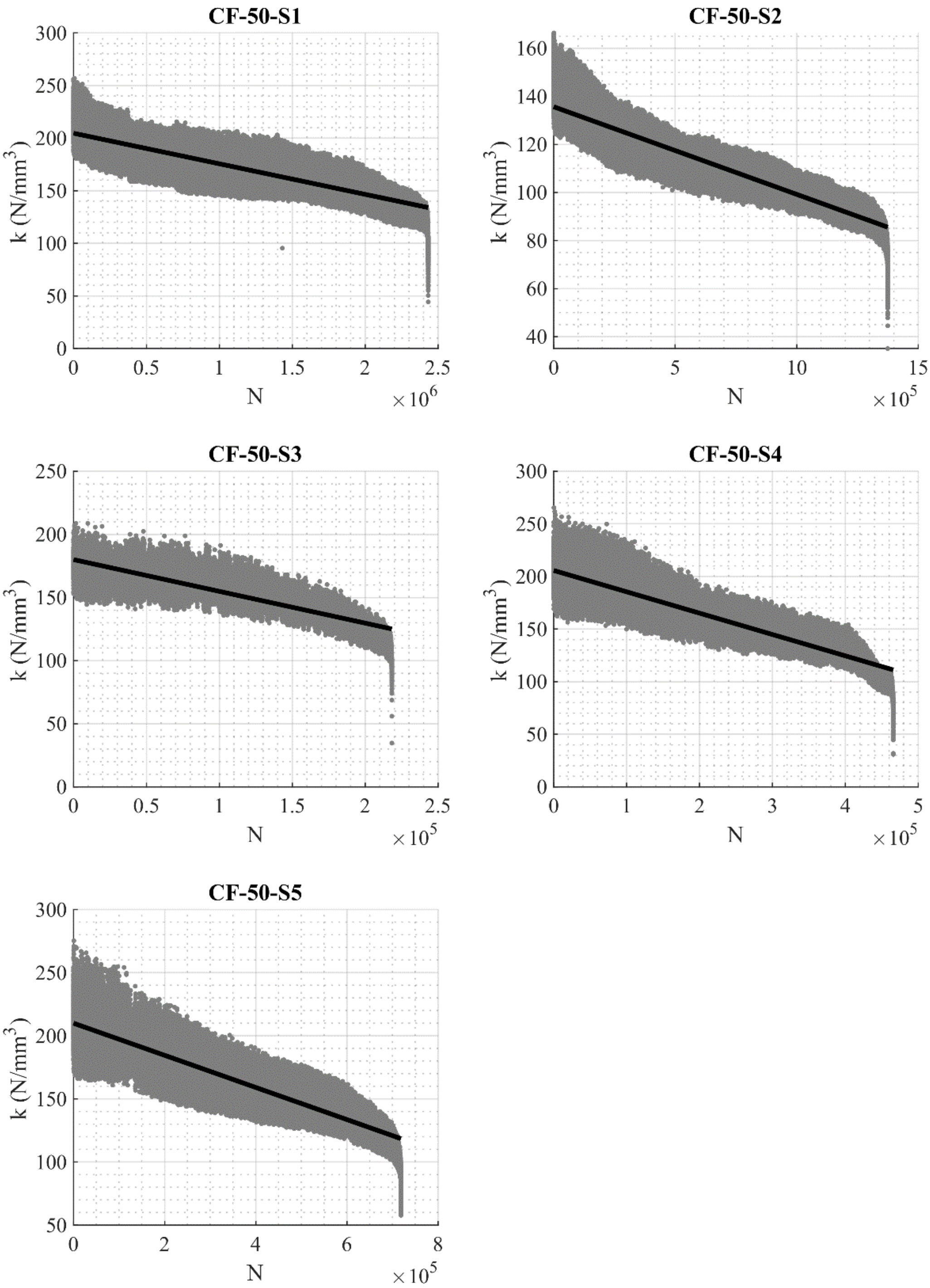

Fig. S20: Variation in cyclic stiffness 50% range (cycled to failure)

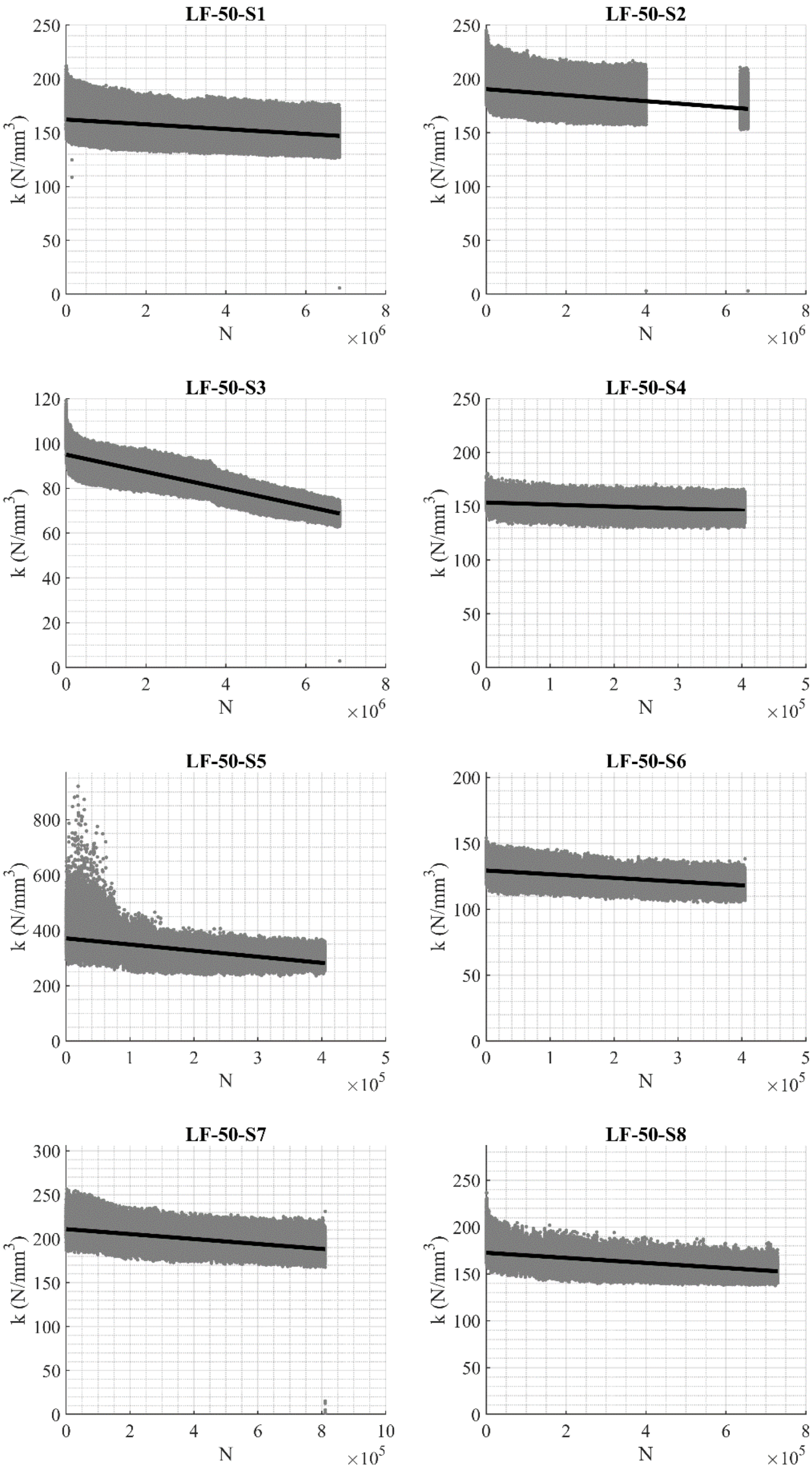

Fig. S21: Variation in cyclic stiffness 50% range (loaded to failure, specimens 1-8)

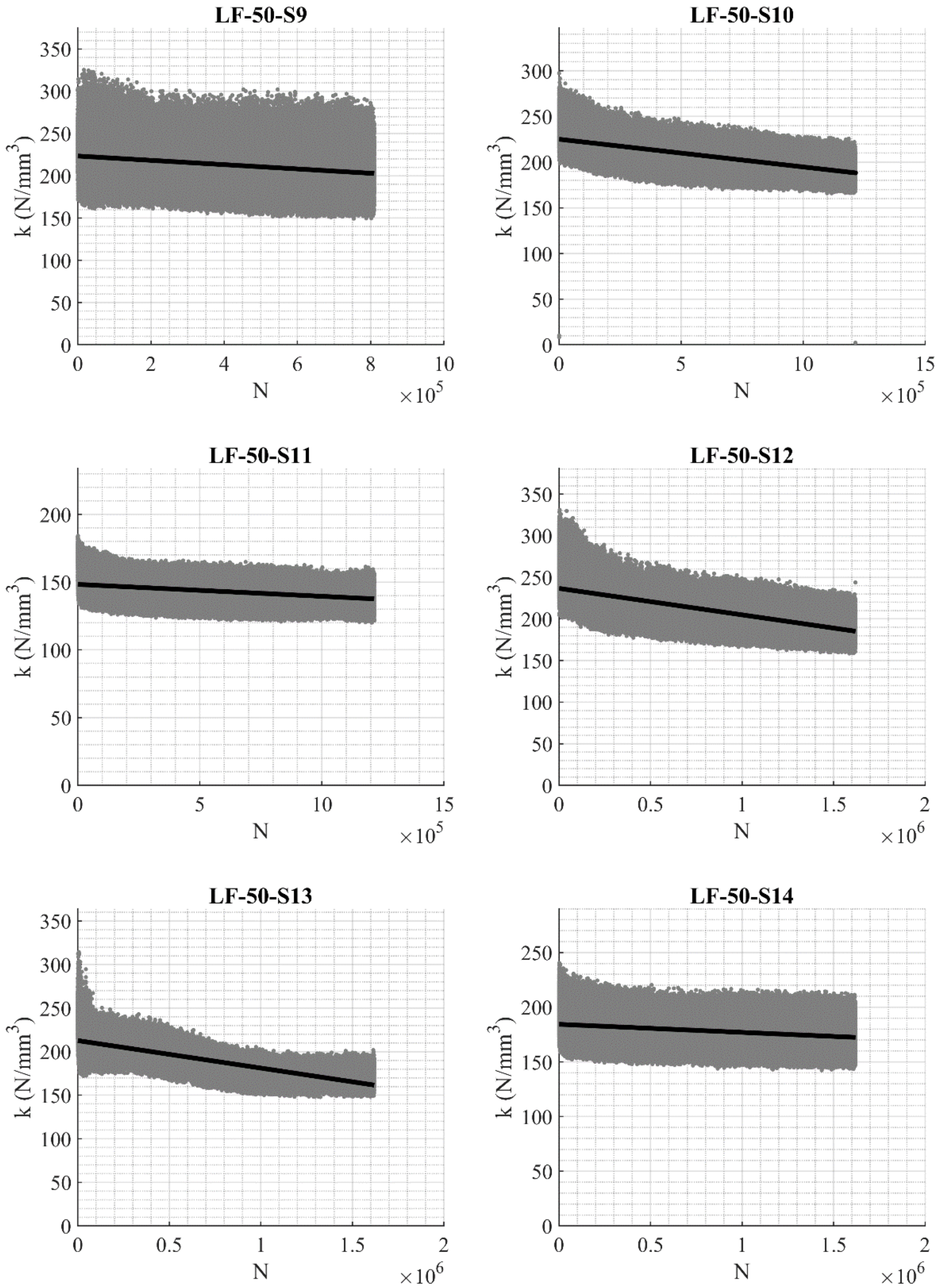

Fig. S22: Variation in cyclic stiffness 50% range (loaded to failure, specimens 9-14)

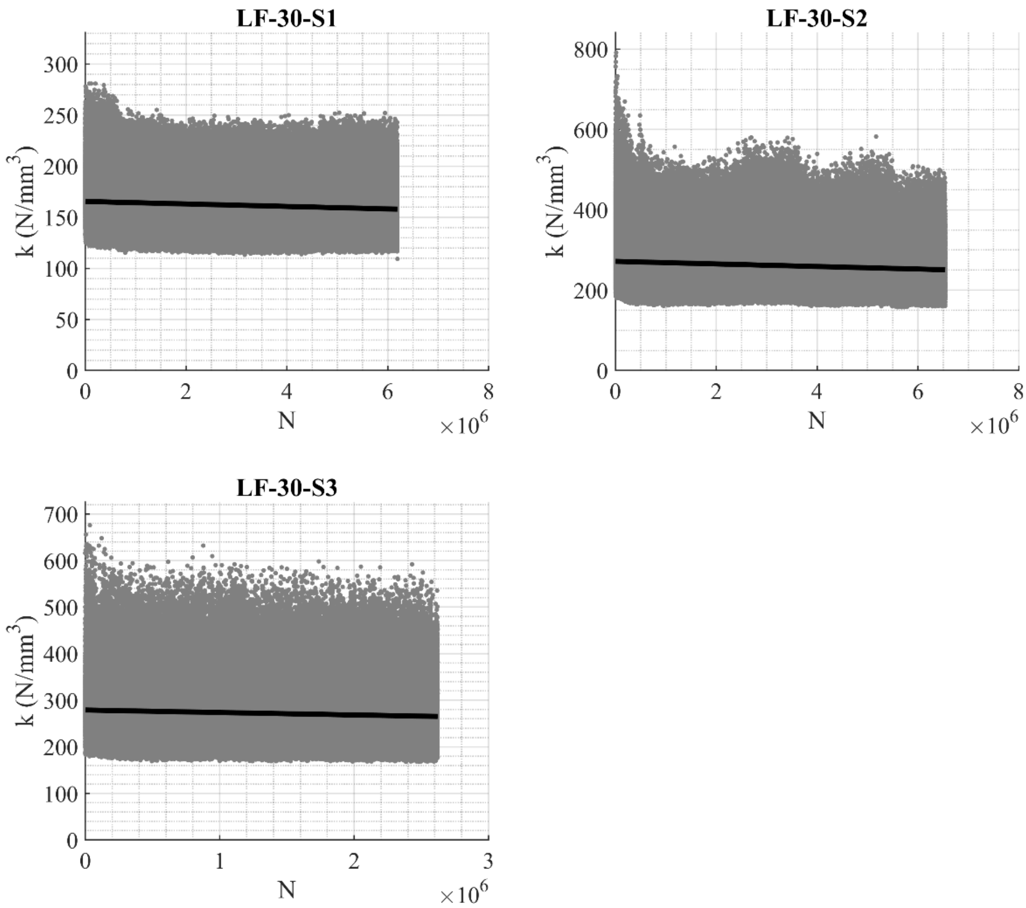

Fig. S23: Variation in cyclic stiffness 30% range